ADVANCING EARTH AND SPACE SCIENCES

JGR Biogeosciences

RESEARCH ARTICLE
10.1029/2025JG009260

Special Collection:
Exploring Carbon Cycling in Aquatic Ecosystems Using Novel Analytical and Data-Driven Approaches

Carbon Cycle Succession Across a Permafrost Thaw Gradient in Northeastern Alberta as Revealed by $\delta^{13}C$ in Dissolved Solids, Gases, and Particulates in Lakes

J. J. Gibson[1,2], P. Eby[1,2], and A. Jaggi[3]

[1]InnoTech Alberta, Victoria, BC, Canada, [2]Department of Geography, University of Victoria, Victoria, BC, Canada, [3]InnoTech Alberta, Calgary, AB, Canada

Key Points:
- Carbon cycle succession accompanies hydrologic and geochemical evolution in lakes across a discontinuous permafrost thaw gradient
- Isotopes assist to constrain roles of thaw-related carbon loading, methanogenesis, methane oxidation, carbonate dissolution processes
- Carbon fractions and isotopic signatures evolve under permafrost thaw with often distinct differences in post-thaw lakes

Supporting Information:
Supporting Information may be found in the online version of this article.

Correspondence to:
J. J. Gibson,
John.Gibson@innotechalberta.ca

Citation:
Gibson, J. J., Eby, P., & Jaggi, A. (2026). Carbon cycle succession across a permafrost thaw gradient in northeastern Alberta as revealed by $\delta^{13}C$ in dissolved solids, gases, and particulates in lakes. *Journal of Geophysical Research: Biogeosciences*, *131*, e2025JG009260. https://doi.org/10.1029/2025JG009260

Received 9 JUL 2025
Accepted 5 JAN 2026

Abstract $\delta^{13}C$ in particulate organic carbon (POC), dissolved organic carbon (DOC), dissolved inorganic carbon (DIC), carbon dioxide ($CO_{2(g)}$) and methane ($CH_{4(g)}$), together with geochemical modeling, were applied to describe carbon cycle evolution in 40 boreal lakes situated across a permafrost thaw gradient in northeastern Alberta, Canada, where hydrological and geochemical trends had previously been established in a multi-decadal study. Progressive carbon cycle succession, characterized by enhanced allochthonous carbon loading, methanogenesis, methane oxidation, and alteration of in-lake DIC regulation, is found to progress in response to periodic water input increases associated with permafrost thaw, and has resulted in modification of the carbon cycle processes in post-thaw lakes. Hydrologic indicators, including water yield (WY), groundwater—surface water ratio (GW/SW), and tritium content appear to undergo evolution across the thaw gradient, and proceed consistently among softwater, circumneutral, and hardwater lakes, although site-specific differences in underlying organic versus inorganic carbon source balances are apparent. Progressive CO_2 supersaturation and CH_4 increases generally accompany permafrost thawing. Isotopic signatures suggest mainly acetoclastic methane production, found in previous studies to be common for newly-thawed peatlands, subsequently modified by methane oxidation in 50% of lakes. Alteration of hydrologic, geochemical and carbon cycling processes has important implications for understanding potential trajectories of climate-driven changes near the southern margin of the zone of discontinuous permafrost.

Plain Language Summary This study forms part of a two-decade investigation of water chemistry of 50 lakes in northeastern Alberta, Canada, seeking to improve understanding of regional water quantity and water quality changes that are occurring in lakes. Here, we investigate the potential role of observed permafrost thaw and its effects on carbon cycling, which evidently includes enhanced input of carbon from thawing peatlands and an apparent increase in methane gas emissions from lakes. Permafrost-related changes may be masking detection of changes occurring due to oil sands industrial development across the region.

1. Introduction

Progressive alteration of the water and carbon cycles in lakes and watersheds under thawing permafrost, coupled with wildfires, has been widely observed across the northern and high-altitude regions (Biskaborn et al., 2019; C. M. Gibson et al., 2018; in't Zandt et al., 2020; Li et al., 2023; Olefeldt et al., 2021; Sun et al., 2022; Vonk et al., 2015; Walvoord & Streigl, 2021), although relatively few studies have examined impacts at the southern limit of discontinuous permafrost, where permafrost becomes fragmented, isolated and/or relict and therefore is particularly vulnerable to temperature changes (Spence et al., 2020; Wright et al., 2022). Permafrost contains an estimated one-third of the world's soil organic carbon, extending across much of the boreal forest and arctic biomes, and covering one-quarter of the northern hemisphere (Meredith et al., 2019; Ogden et al., 2023; E. A. G. Schuur et al., 2015; Walvoord & Streigl, 2021). Physical, chemical and biological responses to climate change and permafrost thaw in boreal and arctic systems have been described in a number of previous studies (e.g., R. M. Holmes et al., 2013; Jorgenson et al., 2013; E. A. G. Schuur et al., 2018, 2022; T. Schuur & Hugelius, 2016; Turetsky et al., 2019; Walvoord & Kurylyk, 2016; Walvoord & Striegl, 2007; Walvoord et al., 2012). In general, temperature and precipitation act as gradual disturbances that directly affect carbon stocks and fluxes and indirectly modify physical processes such as fire, drought, soil subsidence, and erosion and biological processes such as photosynthesis and respiration (E. A. G. Schuur et al., 2018).

Water cycle responses to thawing can be described as heterogeneous for watersheds across the permafrost zone. Previous studies have observed or predicted thaw-associated water yield increases (Bennett et al., 2023; Feng et al., 2021; Zastruzny et al., 2023) water declines (Smith et al., 2005; Webb et al., 2022) or temporal flushing (J. J. Gibson et al., 2019), as well as alteration in seasonality of flows due to interplay between modified hydrologic drivers and geographical sources regions (Peters et al., 2022). In all cases, these studies appear to capture water release and recession of thaw sources, although specific findings appear to have been strongly influenced by the temporal window of investigation, and the geographic extent of each assessment.

Peatland inventories extending across northern Alberta have shown that permafrost occurs in latitudinally-oriented bands, predominantly in peat plateaus such as the Caribou Mountains and Birch Mountains in the north, and as sporadic, treed permafrost mounds within localized peatlands in the south (Beilman et al., 2000). Peatlands began to accumulate carbon in northeastern Alberta around 9,000 years ago and storage rates have fluctuated over time, although they remain a significant carbon sink today (Vitt et al., 2000). Much of the current permafrost present across northeastern Alberta was formed since the Little Ice Age (Vitt et al., 2000), which likely ended in the late 1800s in western Canada (Luckman, 2000), and permafrost is now relict, that is, in disequilibrium with the current climate. Vitt et al. (2000) estimated the areal extent of decline in permafrost to the end of the twentieth century at 9%, whereas recent studies in western Canada have reported declines of 10%–51% locally for wetland-dominated watersheds near the southern limit of discontinuous permafrost (Quinton et al., 2011).

Lake monitoring in northeastern Alberta was initiated by the Regional Aquatics Monitoring Program (RAMP) in 1999, designed primarily to monitor potential acidification of aquatic ecosystems across the oil sands region (e.g., Aherne & Shaw, 2010; Bennett et al., 2008; Curtis et al., 2010; J. J. Gibson et al., 2010; Hatfield Consultants, 2016; Watmough et al., 2014; Whitfield, Aherne, Gibson, et al., 2010; Whitfield, Aherne, Watmough, & McDonald, 2010; WRS, 2006). The RAMP lakes program has provided a consistent, annual record of late summer/fall water quality over several decades in 50 lakes traversing the southern limit of discontinuous permafrost, that has served as a regional hydrochemical benchmark. However, due to the significant and extensive influence of regional permafrost thaw on hydrology and hydrochemistry identified across the oil sands region (e.g., Castrillon-Munoz et al., 2022; J. J. Gibson et al., 2015, 2019, 2020, 2025), and complexity of the landscape which has overwhelmed straightforward monitoring and detection capabilities, acidification effects have been difficult to isolate and/or generally have not been widely observed. A number of paleolimnological investigations have reported similar findings, that is, that climate rather than industrial development has been the predominant driver of regional environmental change over the past century (Curtis et al., 2010; Kurek et al., 2013; Summers et al., 2016; Zabel et al., 2021).

This article presents new analytical results and interpretation based on recent water sampling in 40 RAMP lakes, situated between 55.68°N and 59.72°N and 110.02°W–115.46°W. The lakes span a diverse range of wetland-dominated watersheds, many with isolated or sporadic discontinuous permafrost (Table S1 in Supporting Information S1). Lakes, as receiving water bodies for their surrounding watersheds, and being situated across a gradient in areal permafrost coverage, serve as windows to observe progressive stages in permafrost thaw (J. J. Gibson et al., 2025). We refer to this progression as the "permafrost thaw trajectory," which can be viewed as a conceptual model of spatially juxtaposed landscapes, or as noted by others, as a space-for-time proxy for past and present changes (see Blois et al., 2013; Matveev et al., 2018). In addition to routine geochemical and water isotope sampling, we had an opportunity in 2022 to coordinate collection of water samples for stable carbon isotope analysis, including measurement of $\delta^{13}C$ in particulates (POC) and dissolved species (DIC, DOC, CO_2 and CH_4). We also make reference in our assessment to supporting regional data sets collected within RAMP and other investigations in other years. Aspects of the hydrologic and geochemical changes associated with the thaw transition have been described previously including observed monotonic trends based on Mann-Kendall tau analysis (J. J. Gibson et al., 2015, 2019, 2020, 2025, see also Castrillon-Munoz et al., 2022). Mann-Kendall is a non-parametric statistical test often applied to detect monotonic trends (consistently increasing or decreasing) in hydrologic time-series data, by analyzing the signs of differences between data points, indicating strength and direction of a trend (tau values from −1 to +1) and testing statistical significance (p-value) (Salmi et al., 2002).

The rationale for this new scope of work was to test the hypothesis that carbon cycle succession may also be occurring as a consequence of permafrost thaw. Evidence that the carbon cycle is being generally altered includes the observation that 46 of 50 RAMP lakes have undergone systematic increases in pH over the 2002–2017 period, which was been plausibly linked to permafrost thaw effects (J. J. Gibson et al., 2025). By examining isotopic

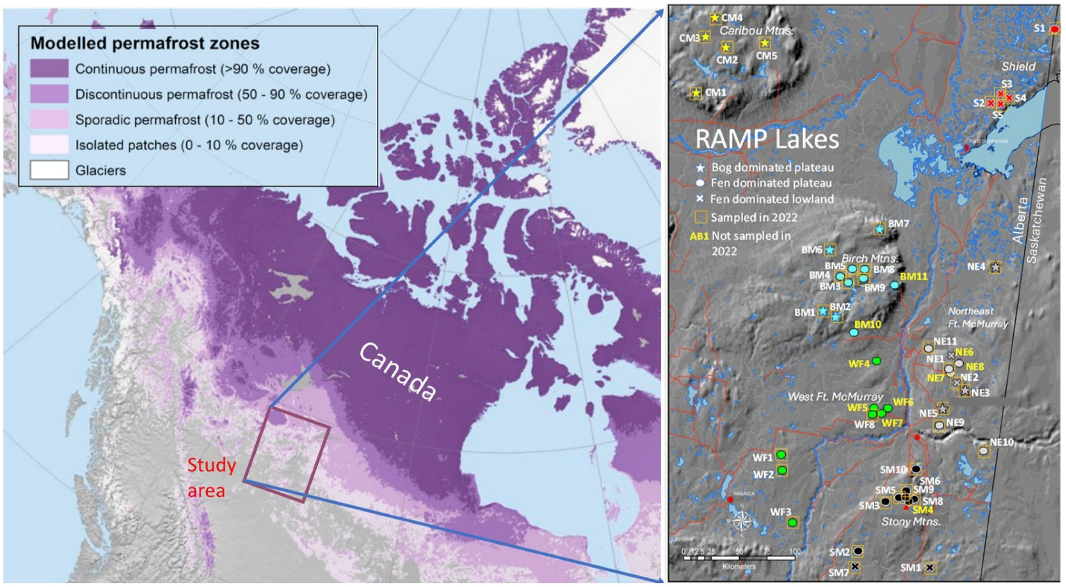

Figure 1. Map of permafrost distribution in North America, with inset showing location of 50 RAMP study lakes, highlighting the 40 lakes sampled in 2022. Study lakes are differentiated by sub-region (colored points) and watershed subtypes, that is, bog dominated plateau, fen dominated plateau and fen dominated lowland (symbols). Vertical exaggeration is used to differentiate plateau regions from lowlands. Blue shading highlights significant regional lakes and incised channels of the Athabasca and Clearwater Rivers (modified from J. J. Gibson et al. (2025); permafrost zones are after Obu et al. (2019)).

indicators of the carbon cycle in lakes at various stages of thaw, we anticipated that we might gain a better understanding of carbon cycle dependence on permafrost thaw impacts, which include effects on water yield to lakes, modification of groundwater/surface water sources, and geochemical fluxes. While this is an important step toward better understanding of heterogeneity in current water quantity and quality across the region, it is also essential for predicting the likely trajectory of change, which has considerable value for sustainable water management within this rapidly developing region.

Changes observed in previous permafrost thaw studies were also of particular interest to our assessment, including allochthonous carbon release from the watershed (R. M. Holmes et al., 2008; Turetsky et al., 2019; Wan et al., 2019, 2020), CO_2 supersaturation in lakes (Castrillon-Munoz et al., 2022; Finlay et al., 2015), methanogenesis (Kuhn et al., 2021; Nydahl et al., 2020) and methane oxidation (Martinez-Cruz et al., 2015). Our aim was to assess the degree to which these factors play a role in carbon cycle alteration and pH adjustment in the RAMP lakes.

2. Study Sites

The Regional Aquatics Monitoring Program (RAMP) was established in 1997 for environmental monitoring to serve the needs of stakeholders in the Regional Municipality of Wood Buffalo (Hatfield Consultants, 2016), the main oil sands development region in Canada and the primary bitumen resource under development worldwide (J. J. Gibson & Peters, 2022). RAMP lakes were selected primarily to assess potential for acidification of lakes under current and projected regional emissions and deposition originating mainly from mining, in situ production and upgrading of bitumen. The network was sampled annually between 1999 and 2017, and following a brief hiatus, continued during 2020–2022 under the aegis of the Joint Oil Sands Monitoring Program (OSM) operated by the governments of Alberta and Canada. Lake sampling has not been carried out during the period between 2023 to the present.

RAMP lakes fall within six distinct geographic sub-regions and span a range in latitude between 55.68° and 59.72°N and longitude between 110.02° and 115.46°W (Figure 1). A subset of 40 lakes was sampled in 2022; 10 lakes being inaccessible during field visits due to unavailability of local helicopter charter services. Collectively, the lakes and their watersheds are considered to be representative of the three main lake-watershed types in the region, that is, bog-dominated permafrost-rich plateau (BDP), fen-dominated plateau (FDP), and fen-dominated lowlands (FDL), where fen-dominated sites are typically permafrost-poor (J. J. Gibson et al., 2025). The sites are mostly headwater lakes and are shallow (i.e., less than 4 m depth), occupying up to 30% of their watershed areas; watersheds varying in size from 57 to 16,555 ha (Table S1 in Supporting Information S1). Additional descriptions of the lakes, watersheds and sub-regions have been provided elsewhere (J. J. Gibson et al., 2015, 2019, 2020, 2025; WRS, 2006). Sub-regions within the Boreal Plains include the Caribou and Birch Mountains (Figure 1), where lakes occur on peat plateaus underlain by permafrost within organic soils overlying surficial tills and low permeability bedrock; the Stony Mountains, which are similar in form but more southerly, and so are largely permafrost free; and intermediate sub-regions including Northeast Ft. McMurray and West Ft. McMurray, which have variable permafrost conditions, variable till thicknesses and bedrock ranging from sandstone, siltstone, or shale to carbonate of Cretaceous to Devonian age. The Shield subregion (Figure 1) is distinct from Boreal Plains subregions owing to its position on the Precambrian Shield, where lakes typically occur within shallow, discontinuous glacial till mantles overlying fractured but relatively impermeable bedrock. Buried erosional channels filled with Quaternary/Tertiary sediments are a common feature of the Boreal Plains subregions, and similar to stream channels, may serve as conduits of inflow or outflow to nearby lakes. Although sampling in 2022 included only 40 of 50 lakes in the network, it extended across all sub-region groups and watershed subtypes, and therefore is considered to be satisfactorily representative of the lakes network as a whole.

The thaw stage classification we apply to RAMP lakes was developed for the 2002–2017 period by J. J. Gibson et al. (2019) based on isotope mass balance of oxygen-18 and deuterium in water ($\delta^{18}O_{H2O}$, $\delta^{2}H_{H2O}$), which differentiated lakes according to four categories: (i) *rising limb*, lakes with above average water yield (WY) observed to be monotonically increasing over the 2002–2017 period (i.e., $WY_{tau} > 0$) (typically with widespread permafrost) (ii) *falling limb*, lakes with above average WY but monotonically decreasing (i.e., $WY_{tau} < 0$) (typically with reduced permafrost coverage) (iii) *recession*, with below average WY that were monotonically decreasing (i.e., $WY_{tau} < 0$) (with sporadic permafrost), and (iv) post thaw, with below average WY but monotonically increasing (i.e., $WY_{tau} > 0$) (with permafrost typically absent).

3. Methods

3.1. Water Sampling

Water quality sampling was carried out by Alberta Environment staff adhering to the protocols outlined in Alberta Environment (2002, 2006) and RAMP (2005). Sampling occurred in late summer (late August/early September) after thermal stratification had ended in most lakes, aiming to capture conditions when lakes were typically well mixed. Lakes were sampled by float plane near the lake centroid employing column-integrated water sampling of the euphotic zone (i.e., surface to Secchi depth) by inserting weighted Tygon tubing outfitted with a one-way valve which was closed to withdraw the sample. This was repeated several times and samples were bulked together. Sampling within 1 m of the lake bottom was avoided. In previous years, smaller lakes which were inaccessible for the float plane were sampled by helicopter. In these cases, 1 L grab samples were collected at 0.5 m below surface. Water samples for geochemical analysis were stored at 4°C until returned for analysis. Samples for oxygen-18 and deuterium analysis were collected in 30 mL high density polyethylene (HDPE) bottles and left unrefrigerated (see J. J. Gibson et al., 2020). Water samples for analysis of carbon-13 in dissolved inorganic carbon (DIC) and dissolved organic carbon (DOC) were field filtered to 0.45μm and collected in separate 30 mL HDPE bottles and kept at 4°C and in darkness until prepared for analysis, which was made within 3 weeks of sampling. Samples for dissolved gas analysis were collected in 500 mL IsoJars™ (Stratum Reservoir [Isotech], Champaign Illinois, USA) which contained an in-built septa in the lid for headspace gas extraction. These samples were also filtered and the filtered material was analyzed for $\delta^{13}C_{POC}$ and $\delta^{15}N_{POM}$.

3.2. Isotopic and Geochemical Analysis

Stable isotopes of water were analyzed according to methods described in J. J. Gibson et al. (2020). Results are provided in "δ" notation in ‰VSMOW, where VSMOW is Vienna Standard Mean Ocean Water. Analytical uncertainty has historically been maintained at better than ±0.2‰ for $\delta^{18}O$ and ±1.0‰ for $\delta^{2}H$ over the course of the RAMP lakes program, and was similarly maintained for the current program.

Stable carbon isotopes in DIC and DOC were analyzed on a Delta V Advantage using a GasBench II peripheral (Assayag et al., 2006). DOC samples were initially acidified and purged with helium to remove any carbonate signature, then an oxidant (sodium persulfate) was added and samples were heated at 80°C for 3 hr, then left to equilibrate overnight before being loaded onto a PAL™ autosampler (CTC Analytics AG (Zwingen, Switzerland)) interfaced with to a Delta V advantage isotope ratio mass spectrometer (IRMS) (Thermofisher, Bremen, Germany). For DIC, samples were added to helium-flushed vials which were then acidified for CO_2 equilibration and similarly loaded onto the autosampler for introduction to the mass spectrometer. Analytical uncertainty is estimated at ±0.3‰ for $\delta^{13}C_{DIC}$ and ±0.4‰ for $\delta^{13}C_{DOC}$. In all cases, $\delta^{13}C$ results are reported in "δ" notation in ‰VPDB, where VPDB is the Vienna PeeDee Belemnite.

$\delta^{13}C$ in particulate organic carbon (POC) was analyzed on filtered material using a Costech 4010 elemental analyzer connected via a Conflo IV to an MAT253 IRMS (Thermofisher, Bremen, Germany). Samples were weighed into tin capsules and then dropped into an oxidation reactor packed with chromium oxide and silvered cobaltous/ic oxide (1020°C). Helium carrier gas was then used to entrain the combustion products through a reduction reactor packed with elemental copper (700°C, to scavenge oxygen and reduce NOx products to N_2) before passing through a water trap (magnesium perchlorate), and a column (to separate N_2 from CO_2), and on to the mass spectrometer. Analytical uncertainty for $\delta^{13}C_{POM}$ is estimated at ±0.2‰.

Dissolved gas samples were prepared by introducing a head space of helium into the IsoJar™ (Isotech, Illinois, USA) then allowing it to equilibrate prior to sampling of the head space for injection into the mass spectrometer. $\delta^{13}C_{CO2}$ and $\delta^{13}C_{CH4}$ were analyzed by GC-IRMS and integrated with a Trace GC Ultra and GC Isolink system connected to the MAT253. Injections were made using a 6-port sampling valve on to a 60m GSQ PLOT column (0.5 mm OD) at 30°C. An oxidation reactor (Pt/Ni) held at 1020°C was employed to convert methane to CO_2 for measurement. Analytical uncertainty for $\delta^{13}C_{CO2}$ and $\delta^{13}C_{CH4}$ is estimated at ±0.2‰. Two methane standards and two carbon dioxide standards were run as samples to establish a scale-adjusted calibration.

Radon-222 (^{222}Rn), a radioactive noble gas used in our case to detect active groundwater sources to lakes (see Arnoux et al., 2017; Petermann et al., 2018), was measured in 37 RAMP lakes in 2010 including 32 lakes included in the 2022 survey. As radon was not measured in 2022, results from 2010 were used in this assessment. RAD7 devices were used to measure ^{222}Rn in the field lab applying a novel canister method (Schmidt et al., 2010), but were later corrected to ensure comparable readings to the standard 2-L polyethylene (PET) pop bottle method (Durridge, 2025). Enriched tritium (^{3}H), a tracer of post-1950s precipitation sources, was previously measured in 19 of the lakes (J. J. Gibson et al., 2016) and these data are likewise included in our assessment.

3.3. Geochemical Modeling

Saturation indices were determined for the RAMP lakes using the equilibrium/mass-transfer model PHREEQC 3.5.0 (Parkhurst & Appelo, 1999) as described in Castrillon-Munoz et al. (2022), with trend analysis reported elsewhere (J. J. Gibson et al., 2025). Saturation indices for calcite (SI calcite) are provided here for lakes sampled in 2022, where $SI > 0$ is indicative of calcite saturation (i.e., potentially precipitating) and $SI < 0$ indicative of calcite undersaturation (i.e., potentially dissolving).

A carbonate speciation calculator described by Helie and Hillaire-Marcel (2006) was used to calculate the distribution of $\delta^{13}C_{CO2}$ and other carbonate species in solution in lake water, accounting for measured temperature, pH, and $\delta^{13}C_{DIC}$. The model is applied to predict $\delta^{13}C_{CO2}$ for the RAMP lakes assuming carbonate equilibrium in exchange with the atmosphere, for comparison with measured values that also may include additional sources such as carbonate dissolution and CH_4 oxidation.

3.4. Statistical Analyses

Mann-Kendall tau and *p* values, applied to assess monotonic trends in climate, water balance and geochemical parameters were calculated with the model of Salmi et al. (2002), as described in J. J. Gibson et al. (2020). Pearson correlations, principal component analysis (PCA), and ANOVA analysis were applied using Sigmaplot 15.0.

3.5. Lake and Watershed Parameters

Physical characteristics for lakes and their watersheds, including latitude, longitude, elevation, lake area, watershed area, lake volume, mean and maximum lake depth, and watershed type classification are provided in Table S1 in Supporting Information S1. Watershed land cover (%) was delimited using 1:18,0000 black and white air photos following the method of Halsey et al. (2003). While 33 land cover categories were differentiated, including many sub-types of wetlands, our analysis here uses the following major classifications: % bog, % fen, % upland, % open-water and % permafrost. Note that time series information on permafrost extent and land cover was unavailable to permit direct analysis of any land cover trends. However, due to differential thaw extent spatially across the region and among study watersheds, particularly across gradients in latitude and elevation, the permafrost thaw gradient concept has been shown to be a useful spatial analog for temporal changes in permafrost thaw effects occurring in lakes across the region (see J. J. Gibson et al., 2019, 2025).

3.6. Climate and Water Balance Analysis

A database compiled by J. J. Gibson et al. (2020) summarizes concurrent annual site-specific climate data and trends interpolated for the RAMP lakes during 2002–2017 based on North American Regional Reanalysis (NARR), a 32-km gridded multi-layer climate data set. Year-specific monthly climate data, including 2-m air temperature, 2-m relative humidity, precipitation (P), open-water evaporation (E) and potential evapotranspiration (ET) at ground surface were interpolated for specific lake locations. Estimates of evaporation-flux-weighted air temperature (T_{fw}) and humidity (h_{fw}) were also calculated and used to run a site-specific isotope mass balance model (J. J. Gibson et al., 2019). Combined with lake and watershed parameters, these were applied to obtain estimates of lake residence time (t) evaporation/inflow (E/I), and water yield (WY) for each lake-watershed system.

3.7. Water Yield, Runoff, and GW/SW

A climatological runoff estimate (RO) from the drainage basin area was approximated based on NARR from the volumetric flux deficit, P–ET, where P is precipitation and ET is evapotranspiration from the catchment, similar to the approach used by J. J. Gibson et al. (2022) for open water wetlands. RO was then used as an estimate of surface runoff and WY - RO was used to approximate groundwater contributions to the lakes. These metrics were then combined to estimate the ratio GW/SW, used as a baseflow index for each lake, as well for computing interannual Mann-Kendall statistics for the period of contiguous annual monitoring (2002–2017).

4. Results and Discussion

Data from the 2022 survey, as well as selected indicators from prior sampling years, are provided in Tables 1 and 2. Table 1 summarizes carbon isotopic data and related geochemical measurements, whereas Table 2 summarizes supporting data including hydrologic characteristics and permafrost thaw stage classification. Supporting data collected in prior years (Tables S2 and S3 in Supporting Information S1) and a Pearson correlation matrix (Table S4 in Supporting Information S1) are also provided as Supporting Information S1.

4.1. Site-Specific Characterization

4.1.1. General Geochemical Patterns

A conceptual model of water and carbon cycle processes summarizes interactions anticipated to be occurring within typical boreal watershed-lake systems in the region, as well as controlling factors such as local hydrostratigraphy, permafrost thaw processes, in-lake regulation mechanisms, and atmospheric exchange (Figure 2). Key tracers used in this and previous assessments are also shown. Geochemical variations for the RAMP lakes were previously described by Castrillon-Munoz et al. (2022). Statistically significant correlations among variables at $p < 0.001$ level (unless otherwise specified) are described here (see also Table S1 in Supporting Information S1). Electrical conductivity (EC), as for total dissolved solids, was found to increase with pH ($r = 0.735$), HCO_3 ($r = 0.972$) and DIC ($r = 0.968$) indicating that carbonate alkalinity is the primary source of dissolved solids. Isotopic values also increased with EC, including $\delta^{13}C_{CO2}$ ($r = 0.689$) and $\delta^{13}C_{DIC}$ ($r = 0.731$) suggesting mainly carbonate dissolution controls. Color was found to decrease with pH ($r = -0.597$) and in relation to $\delta^{13}C_{CO2}$ ($r = -0.676$) and $\delta^{13}C_{DIC}$ ($r = -0.637$), and was positively correlated with DOC (0.373; $p = 0.018$). The productivity indicator chlorophyll-A (Chl-a) increased with turbidity ($r = 0.803$), DOC ($r = 0.666$), DON ($r = 0.688$), and $CO_{2(aq)}$ ($r = 0.648$), and in concert with isotopic indicators of carbon-nutrient sources, $\delta^{13}C_{POC}$ ($r = 0.688$), $\delta^{13}C_{DOC}$ ($r = 0.621$), but with no apparent relationship to methane production, $CH_{4(aq)}$, although apparently having some influence on the isotopic labeling of methane, $\delta^{13}C_{CH4}$ (0.511). We note covariation of $\delta^{13}C_{CH4}$ and $\delta^{13}C_{CO2}$ ($r = 0.560$), which is explored later on in relation to mechanistic causes. $CH_{4(aq)}$ is found to increase both in response to lake surface temperature ($r = 0.383$, $p = 0.015$) and bottom

AGU ADVANCING EARTH AND SPACE SCIENCES

Journal of Geophysical Research: Biogeosciences

10.1029/2025JG009260

Table 1
Gas Concentration and Related Isotopic Values as Measured and Modeled for Lakes Included in the Fall 2022 Survey

	Measured										DIC equilibrium values based on speciation calculator		Calculated apparent isotopic separation
Lake ID	CO_2 (ppm)	$\delta^{13}C_{CO2}$ (‰VPDB)	CH_4 (ppm)	$\delta^{13}C_{CH4}$ (‰VPDB)	POM (ppm)	$\delta^{13}C_{POC}$ (‰VPDB)	DOC (ppm)	$\delta^{13}C_{DOC}$ (‰VPDB)	DIC (ppm)	$\delta^{13}C_{DIC}$ (‰VPDB)	CO_2 (ppm)	$\delta^{13}C_{CO2}$ (‰VPDB)	$\alpha_{CO2\text{-}CH4}$ (‰VPDB)
NE1	3,827	−22.06	125.07	−60.61	2.00	−26.60	26.26	−27.87	0.61	−19.88	802	−23.79	1.0410
NE2	2,228	−21.03	36.62	−66.35	0.00	−31.86	29.04	−28.88	1.44	−15.85	1,135	−23.90	1.0485
NE3	3,094	−16.55	19.65	−56.76	3.00	−29.36	22.10	−27.93	3.77	−9.28	1,336	−20.02	1.0426
NE4	1,848	−17.04	11.04	−57.48	6.00	−30.01	15.22	−28.48	2.61	−11.63	1,230	−21.84	1.0429
NE5	5,002	−13.38	33.56	−14.16	19.00	−25.06	39.25	−27.36	3.55	−9.68	1,045	−21.04	1.0008
NE9	2,807	−9.73	108.43	−32.29	2.00	−27.90	27.07	−26.81	14.26	−1.51	558	−13.61	1.0233
NE10	3,352	−4.29	1.92	11.15	9.00	−23.66	23.55	−25.74	13.81	3.21	265	−8.39	0.9847
NE11	4,629	−13.90	160.71	−49.49	3.00	−29.86	25.13	−27.93	18.15	−5.86	647	−18.57	1.0374
SM1	1,590	−10.95	106.54	−23.58	2.00	−25.82	22.91	−25.94	3.29	−5.27	813	−16.51	1.0129
SM2	2,322	−18.82	87.93	−41.57	4.00	−24.30	25.04	−26.28	1.31	−16.83	886	−26.19	1.0237
SM3	1,570	−19.04	74.98	−53.57	1.00	−29.89	12.64	−28.38	0.93	−12.41	704	−20.74	1.0365
SM5	2,113	−25.20	22.28	−48.08	2.00	−30.15	15.24	−28.45	0.68	−23.95	985	−27.34	1.0240
SM6	2,179	−25.35	32.46	−54.57	3.00	−29.38	15.42	−27.87	0.37	−23.55	617	−24.98	1.0309
SM7	1,902	−20.19	40.43	−33.25	1.00	−30.10	17.92	−27.81	1.52	−15.46	996	−24.79	1.0135
SM8	2,111	−25.88	25.43	−52.76	5.00	−30.79	14.69	−28.27	0.40	−24.66	714	−25.43	1.0284
SM9	2,262	−26.49	23.22	−53.78	2.00	−31.88	20.10	−28.25	0.34	−26.57	611	−26.94	1.0288
SM10	1,660	−24.46	12.26	−58.73	2.00	−31.74	19.73	−28.06	0.37	−24.44	669	−25.02	1.0364
WF1	6,346	−15.48	10.97	46.69	8.00	−17.95	43.75	−21.24	3.41	−11.51	1,235	−22.56	0.9406
WF2	3,430	−23.11	36.75	−59.81	0.00	−29.57	20.08	−27.82	1.98	−18.87	1,371	−28.27	1.0390
WF3	2,666	−25.75	44.82	−55.40	3.00	−31.70	34.86	−29.14	0.50	−26.14	890	−26.96	1.0314
WF8	1,793	−10.79	9.42	39.66	3.00	−27.12	23.34	−27.03	8.08	−3.45	690	−15.50	0.9515
BM1	1,739	−16.44	7.10	−60.59	1.00	−29.74	8.43	−27.00	2.37	−9.67	972	−20.11	1.0470
BM2	1,693	−14.07	3.82	−51.25	0.00	−26.70	7.94	−26.15	5.04	−5.05	995	−16.51	1.0392
BM3	4,272	−19.28	28.24	−65.19	0.00	−28.78	20.84	−27.56	2.94	−14.53	817	−26.58	1.0491
BM4	2,712	−18.07	5.72	−63.04	7.00	−28.32	22.71	−27.51	3.31	−11.89	1,636	−21.92	1.0480
BM5	4,179	−25.37	10.26	−60.37	3.00	−29.34	23.10	−27.21	1.18	−19.85	958	−28.02	1.0372
BM6	4,182	−27.98	10.01	−54.86	2.00	−29.37	27.83	−27.75	0.44	−24.75	732	−25.86	1.0284
BM7	2,904	−25.64	10.99	−50.97	9.00	−30.38	19.89	−28.87	0.49	−27.76	833	−27.88	1.0267
BM8	6,122	−21.69	17.89	−66.04	17.00	−27.17	24.57	−27.22	2.03	−14.21	1,069	−24.25	1.0475
BM9	2,665	−19.00	8.39	−47.25	0.00	−29.89	13.67	−27.67	1.68	−16.70	837	−27.22	1.0297
CM1	1,585	−17.68	1.57	−54.07	0.00	−30.61	21.83	−26.83	4.74	−9.82	1,125	−21.43	1.0385
CM2	3,162	−18.58	3.68	−67.63	0.00	−30.53	14.12	−26.95	2.25	−13.67	939	−24.14	1.0526
CM3	3,365	−20.05	28.54	−58.42	3.00	−29.35	22.13	−27.34	2.10	−16.18	907	−26.69	1.0408
CM4	2,568	−19.65	1.31	−54.05	0.00	−29.69	22.23	−27.08	1.65	−15.22	849	−25.09	1.0364
CM5	4,776	−23.79	34.55	−65.06	2.00	−30.60	22.25	−27.37	1.19	−21.35	909	−29.42	1.0441
S1	1,523	−12.07	3.77	−48.14	0.00	−28.60	10.14	−26.01	5.47	−4.84	876	−16.52	1.0379
S2	1,821	−20.32	7.74	−54.40	1.00	−31.38	19.34	−28.02	4.09	−13.73	1,119	−25.76	1.0360
S3	1,459	−17.32	4.72	−49.33	5.00	−31.34	16.17	−28.05	3.49	−10.60	928	−22.25	1.0337
S4	2,457	−17.27	30.15	−64.36	0.00	−30.60	14.26	−27.96	5.03	−10.78	837	−23.22	1.0503
S5	3,981	−16.89	42.27	−34.40	6.00	−28.20	23.11	−28.39	2.55	−13.88	1,001	−24.93	1.0181

Table 2
Water Isotope Data for 2022 and Long-Term (2002–17) Estimates of Hydrologic Parameters for Lakes Sampled in the 2022 Survey

Lake ID	δ^2H (‰VSMOW)	δ^{18}O (‰VSMOW)	WY (mm/yr)	WY_{tau}	E/I	GW/SW	GW/SW_{tau}	*t* (years)	Thaw stage classification
NE1	−125.63	−14.19	181	−0.150	0.128	0.214	0.225	0.563	3
NE2	−126.47	−14.16	108	−0.283	0.118	0.000	0.175	0.549	3
NE3	−115.48	−12.67	137	−0.017	0.186	0.000	0.092	0.420	3
NE4	−124.42	−13.70	500	−0.250	0.180	8.448	0.058	1.116	2
NE5	−104.10	−10.39	442	0.200	0.328	6.703	0.325	1.064	1
NE9	−98.75	−9.52	318	0.067	0.427	2.623	0.325	1.668	1
NE10	−99.15	−9.44	245	−0.167	0.448	1.928	0.358	1.214	4
NE11	−112.96	−11.57	135	−0.167	0.282	0.333	0.038	1.377	3
SM1	−97.91	−9.52	255	0.217	0.459	2.020	0.325	1.032	1
SM2	−98.61	−9.41	93	0.050	0.505	0.000	0.142	1.006	4
SM3	−106.76	−10.91	319	−0.200	0.388	0.207	0.025	1.964	1
SM5	−105.43	−10.55	369	0.233	0.404	0.145	0.042	1.630	1
SM6	−108.63	−11.17	77	0.233	0.315	0.000	0.108	0.974	4
SM7	−101.40	−9.89	222	0.100	0.434	0.000	0.142	1.930	1
SM8	−107.53	−11.04	287	0.317	0.357	0.000	0.142	1.107	1
SM9	−114.44	−12.21	286	0.133	0.248	0.000	0.175	0.492	1
SM10	−118.15	−12.87	157	0.267	0.243	0.000	0.125	0.588	4
WF1	−99.30	−9.47	302	0.383	0.492	0.000	0.058	1.022	4
WF2	−98.58	−9.27	122	0.233	0.541	0.000	0.092	1.774	4
WF3	−104.87	−10.69	63	0.283	0.333	0.000	0.058	1.101	4
WF8	−106.30	−10.62	72	0.217	0.459	0.000	0.152	1.152	4
BM1	−118.76	−13.51	618	0.100	0.261	1.511	−0.142	5.774	1
BM2	−112.75	−12.36	511	0.183	0.278	4.140	−0.208	10.807	1
BM3	−136.44	−15.55	114	0.117	0.140	0.000	−0.242	0.777	2
BM4	−121.17	−12.92	250	0.133	0.229	0.997	−0.208	0.393	2
BM5	−127.10	−14.18	216	0.300	0.203	1.016	−0.208	0.371	2
BM6	−139.58	−16.38	460	0.067	0.123	5.130	−0.108	0.222	3
BM7	−126.61	−14.30	365	0.150	0.206	0.000	−0.308	0.547	2
BM8	−126.70	−14.28	156	0.371	0.122	0.623	−0.142	0.559	4
BM9	−134.54	−16.13	285	0.283	0.170	1.518	−0.175	2.228	1
CM1	−139.88	−16.94	468	0.467	0.084	2.004	−0.038	1.990	1
CM2	−132.34	−15.37	371	−0.067	0.230	3.049	−0.057	3.108	1
CM3	−139.00	−16.28	258	−0.083	0.153	15.910	0.019	1.117	1
CM4	−146.08	−17.76	311	−0.067	0.101	0.000	−0.019	3.735	1
CM5	−124.31	−13.17	307	−0.083	0.292	1.973	−0.171	2.105	3
S1	−120.88	−13.29	435	−0.367	0.278	523[a]	−0.108	7.801	1
S2	−143.11	−12.18	44	0.033	0.096	0.000	−0.019	1.443	3
S3	−134.03	−15.62	132	0.233	0.129	3.609	−0.275	1.848	3
S4	−131.43	−14.99	32	0.017	0.168	0.845	−0.025	2.860	3
S5	−122.69	−13.16	103	0.217	0.279	2.181	−0.038	1.172	3

Note. WY is water yield; WY_{tau} is long-term trend in water yield from J. J. Gibson et al. (2019) used in the thaw stage classification: (1) rising limb, (2) falling limb, (3) recession, (4) post thaw; E/I is ratio of evaporation to inflow; GW/SW is ratio of groundwater to surface water, and GW/SW_{tau} is long-term trend in ratio of groundwater to surface water. *t* is estimated lake residence time based on isotope mass balance. [a]Not plotted in Figure 8.

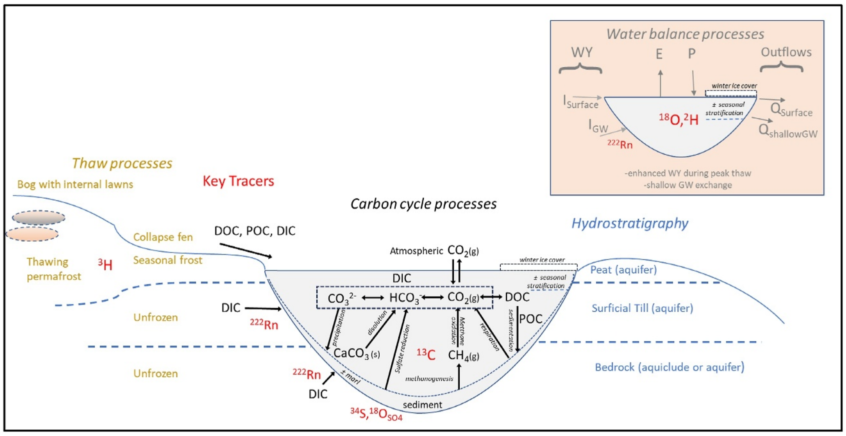

Figure 2. Schematic showing typical watershed characteristics (thaw processes, hydrostratigraphy) and lake features (sedimentation, ice cover, stratification) influencing carbon cycle processes in lakes including key tracers. Inset summarizes associated lake water balance processes and key tracers. Interaction of various in-lake carbon reservoirs and fluxes are highlighted for a typical lake. DOC and DIC are dissolved organic and inorganic carbon, respectively; POC is particulate organic carbon; DIC species include: carbonate CO_3^{2-}, bicarbonate, HCO_3^- and carbon dioxide CO_2. WY is water yield, $I_{surface}$ and I_{GW} are surface and subsurface inflow, $Q_{surface}$ and Q_{GW} are surface and subsurface outflow; ^{18}O, ^{2}H, and ^{3}H are oxygen-18, deuterium and enriched tritium in water, respectively; ^{222}Rn is dissolved radon gas; ^{34}S, $^{18}O_{SO4}$ refer to sulfur-34 and oxygen-18 in sulfate, which were not applied here, but may be informative for characterizing coupling with the sulfur cycle via sulfate reduction in lake sediments.

temperature ($r = 0.486$, $p = 0.001$), although a stronger dependency is noted for the latter. Isotopic indicators of carbon-nutrient sources, $\delta^{13}C_{POC}$ and $\delta^{13}C_{DOC}$, were found to be highly covariant ($r = 0.846$). Interdependence was also noted between $\delta^{13}C_{DIC}$ and $\delta^{13}C_{CO2}$ ($r = 0.965$), and to some extent, $\delta^{13}C_{DOC}$ ($r = 0.455$, $p = 0.003$) and $\delta^{13}C_{CH4}$ ($r = 0.445$, $p = 0.004$).

One test of the significance of respiration and primary production in $\delta^{13}C_{DIC}$ regulation, as suggested by de Kluijver et al. (2014), is strength of a negative correlation between $\delta^{13}C_{DIC}$ and $CO_{2(aq)}$ in the case of respiration control, and positive correlation in the case of primary production control. We find only a weak, insignificant relationship between these variables ($r = -0.061$, $p = 0.709$), suggesting that they are not primary drivers of $\delta^{13}C_{DIC}$ variability across the RAMP lakes network. Rather, $\delta^{13}C_{DIC}$ appears to be controlled mainly by carbonate dissolution which also depends on hydrologic flushing, and potentially by secondary processes such as methanogenesis and methane oxidation, as discussed later on. Furthermore, we infer that $\delta^{13}C_{POC}$ and $\delta^{13}C_{DOC}$ are primarily indicators of allochthonous carbon-nutrient loads to the lakes, with high covariance between these indicators suggesting the dominance of allochthonous over pelagic sources in most lakes. Controlling factors do not appear to be significantly influenced by proximity to oil sands industrial activity, which has been noted in previous descriptions of hydrologic and geochemical variations in the lakes (Bennett et al., 2008; J. J. Gibson et al., 2010, 2015, 2019, 2025) and various paleolimnological assessments (Curtis et al., 2010; Kurek et al., 2013; Summers et al., 2016; Zabel et al., 2021).

4.1.2. CO_2 and CH_4

Dissolved CO_2 sampled in the lakes was found to range from 1,459 to 6,346 ppm, with a wide range in measured $\delta^{13}C_{CO2}$ values between −27.58 and −4.29 ‰VPDB. In comparison, values from the carbonate speciation calculator of Helie and Hillaire-Marcel (2006) predicted CO_2 and $\delta^{13}C_{CO2}$ to range from 265 to 1,636 ppm and from −29.42 to −8.39 ‰VPDB, respectively, assuming DIC equilibrium with the atmosphere. Measured values for CO_2 were evidently much higher indicating CO_2 supersaturation, as suggested previously for the RAMP lakes based on PHREEQC geochemical modeling (Castrillon-Munoz et al., 2022). Calculated values of $\delta^{13}C_{CO2}$ varied widely depending on pH, alkalinity and relative water softness. Excess $CO_{2\,(aq)}$ (observed - calculated equilibrium CO_2; Table 1) was found to be moderately correlated with EC ($r = 0.516$) and $\delta^{13}C_{POC}$ (0.411) as well as DIC ($r = 0.492$, $p = 0.001$), DOC ($r = 0.389$, $p = 0.013$), and POM ($r = 0.382$, $p = 0.015$), which we infer to reflect interaction of a combination of underlying factors including carbonate dissolution and allochthonous loading.

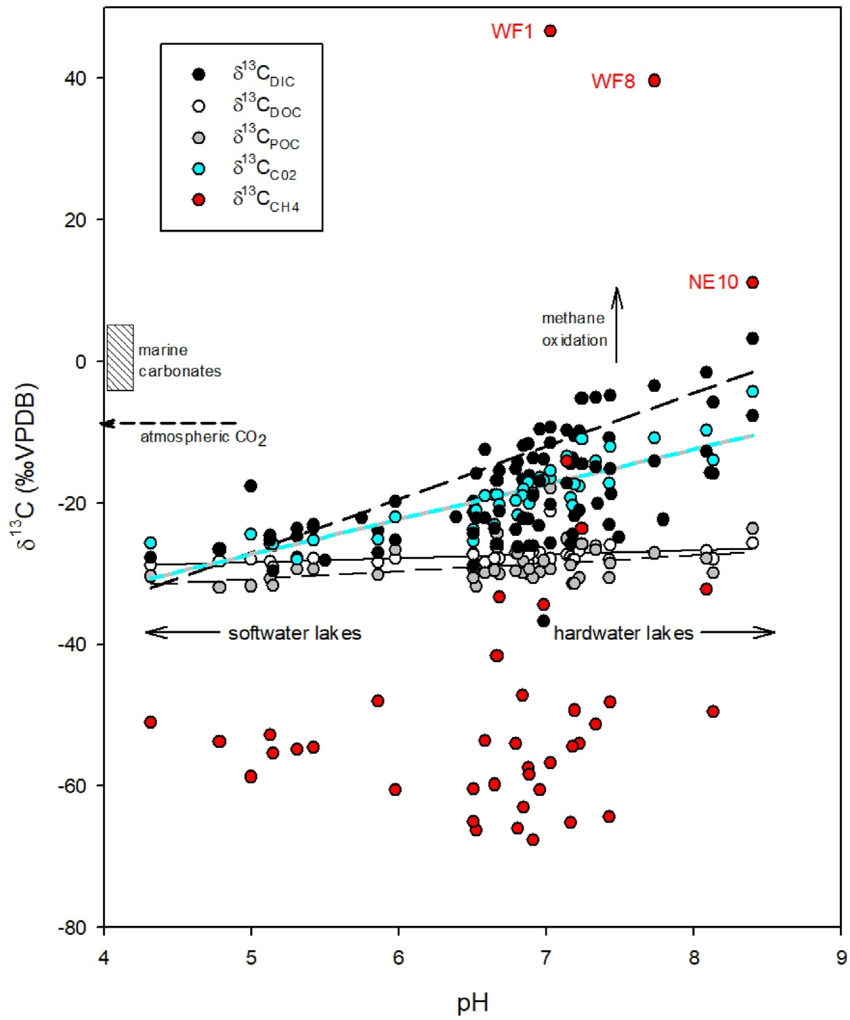

Figure 3. Relationship between pH and carbon-13 signatures for primary carbon cycle components sampled in lakes in 2022 (with lines showing correlations, see Table S4 in Supporting Information S1). $\delta^{13}C$ reference values are shown for marine carbonates and 2015 atmospheric CO_2 based on Saltzman and Thomas (2012) and Graven et al. (2020), respectively. Variation in carbon-13 signatures in DIC mainly reflect lake-specific balance of biogenic CO_2 versus carbonate dissolution controls, as modified by CO_2 exchange, methanogenesis and potentially by other processes shown in Figure 2. While carbon-13 in methane is reflective of acetoclastic fermentation in lake bottom sediments, the enrichment of $\delta^{13}C_{CH4}$ by methane oxidation in the water column is also occurring in many lakes. Lakes with extreme methane enrichment are labeled by lake ID.

Systematic variations in $\delta^{13}C_{CO2}$ with pH (Figure 3) in relation to $\delta^{13}C_{DIC}$, $\delta^{13}C_{DOC}$, $\delta^{13}C_{POC}$ and more variable isotopic signatures of $\delta^{13}C_{CH4}$, attest to strong control of carbonate equilibria somewhat decoupled from methanogenesis. CH_4 and $\delta^{13}C_{CH4}$ are found to be better correlated with bottom versus top temperatures in the lakes (Table S4 in Supporting Information S1), and for some lakes, $\delta^{13}C_{CH4}$ is inferred to be enriched due to methane oxidation, likely occurring in the water column. Previous studies have described considerable spatial and temporal variability in CO_2 and CH_4 in small boreal lakes (e.g., Denfeld et al., 2020), however, our data collection was limited to one-time sampling of the euphotic zone after the time of fall turnover and at or close to the lake centroid. Despite this limitation, we find results to be useful for site-to-site comparisons. Based on the $\delta^{13}C_{CO2}$ versus $\delta^{13}C_{CH4}$ classification (Milkov & Etiope, 2018; Whiticar et al., 1986) (Figure 4), the mechanism of methane generation for all lakes is consistent with acetoclastic fermentation, found to be more common for newly thawed bogs than mature bogs (see Heffernan et al., 2021), with enrichment in $\delta^{13}C_{CH4}$ relative to $\delta^{13}C_{CO2}$ being consistent with methane oxidation (Milkov & Etiope, 2018; Whiticar et al., 1986). As opposed to data sets obtained from multiple northern peatlands (see Heffernan et al., 2021; M. E. Holmes et al., 2015), we see no isotopic

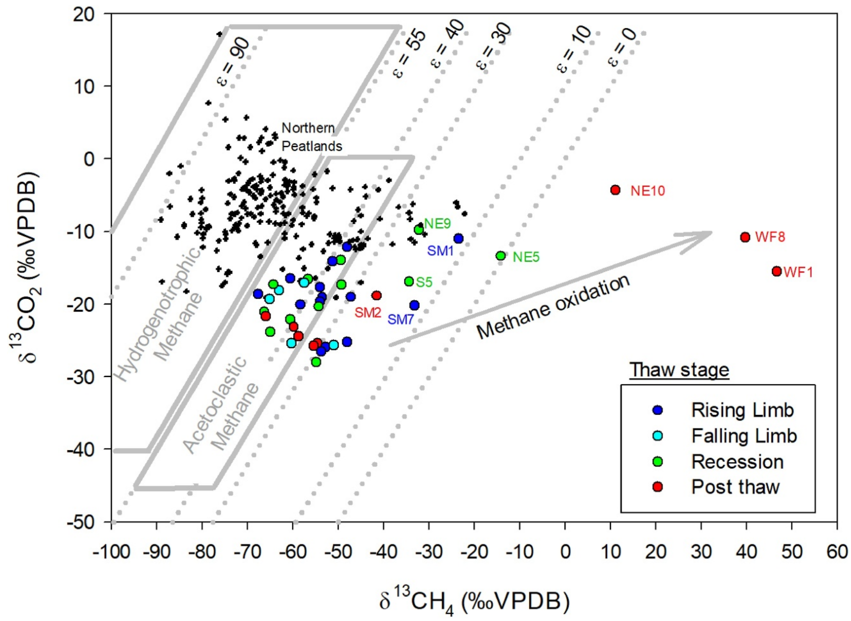

Figure 4. Crossplot of carbon-13 signatures in carbon dioxide and methane in study lakes, classified by thaw status according to J. J. Gibson et al. (2019) (see legend). Reference ranges and isotopic separations (ε) are consistent with Whiticar et al. (1986). Comparative field data for northern peatlands (black crosses) are compiled from M. E. Holmes et al. (2015) and Heffernan et al. (2021). Methane generation across the thaw gradient appears to reflect acetoclastic fermentation pathways, with alteration by methane oxidation ($\alpha > 1.035$) evident in approximately half of the lakes (18 of 40). Selected lakes are identified by lake ID.

signatures present indicating methanogenesis by hydrogenotrophic (CO_2 reduction) mechanisms (Figure 4). Heavy isotope enrichment due to methane oxidation is found to be greatest in three post-thaw lakes, but this process appears to be active in about 18 of 40 lakes (based on criteria $\alpha > 1.035$; Figure 4), including lakes at all thaw stages. Previous studies have shown CO_2 generation to be widely occurring in area wetlands (Whitfield et al., 2009) although prediction of CO_2 in lake water was found to be dependant on other factors regulating in-lake CO_2. The differentiation of impacts from allochthonous carbon sources versus effects of methanogenesis on $\delta^{13}C_{DIC}$ was somewhat more difficult to assess, as discussed later on.

4.1.3. DOC, DIC, POC

For hardwater lakes, $\delta^{13}C_{DIC}$ is enriched but systematically tracks $\delta^{13}C_{CO2}$ (Figure 3), but transitions to being more depleted than $\delta^{13}C_{CO2}$ and more consistent with $\delta^{13}C_{DOC}$ for softwater lakes (pH < 6.5), which are known to be buffered primarily by carboxylic acids (see Castrillon-Munoz et al., 2022). Overall, this pattern of $\delta^{13}C_{CO2}$ and $\delta^{13}C_{DIC}$ variation is attributed to the relative influence of inorganic versus organic carbon sources, the latter being prevalent for softwater lakes. $\delta^{13}C_{DOC}$ and $\delta^{13}C_{POC}$ are found to be similar and largely invariant across the entire pH range, with terrestrial signatures in most cases within the range of −27‰ to −30 ‰VPDB, as found in modern C3 plants in the region (see Marwick et al., 2015). Such values are consistent with observations from numerous freshwater studies (e.g., Helie & Hillaire-Marcel, 2006), and are a clear indication of POC degradation and/or biotic synthesis. Exceptions are noted for eutrophic lakes (WF1, NE10, NE5) which are characterized by high POC, high CO_2-excess, and anomalously enriched $\delta^{13}C_{DOC}$ (up to −21.24 ‰VPDB) and $\delta^{13}C_{POC}$ (up to −17.95 ‰VPDB). Methane oxidation is also characteristic of these lakes. Carbon cycling processes were generally found to be consistent with our overall conceptual model (Figure 2).

4.1.4. Allochthonous Sources

Measured values for $\delta^{13}C_{POC}$ and $\delta^{15}N_{POM}$ were found to be similar in both 2021 ($n = 50$) and 2022 ($n = 40$) (Figure 5), and comparable to values obtained from an unpublished 2009 survey of 125 lakes in the Southern Athabasca region, centered on the Stony Mountains. POM isotope signatures were also consistent with a nearby lake survey in boreal forest terrain southwest of the study area (Beaudoin et al., 2001), but our data set showed

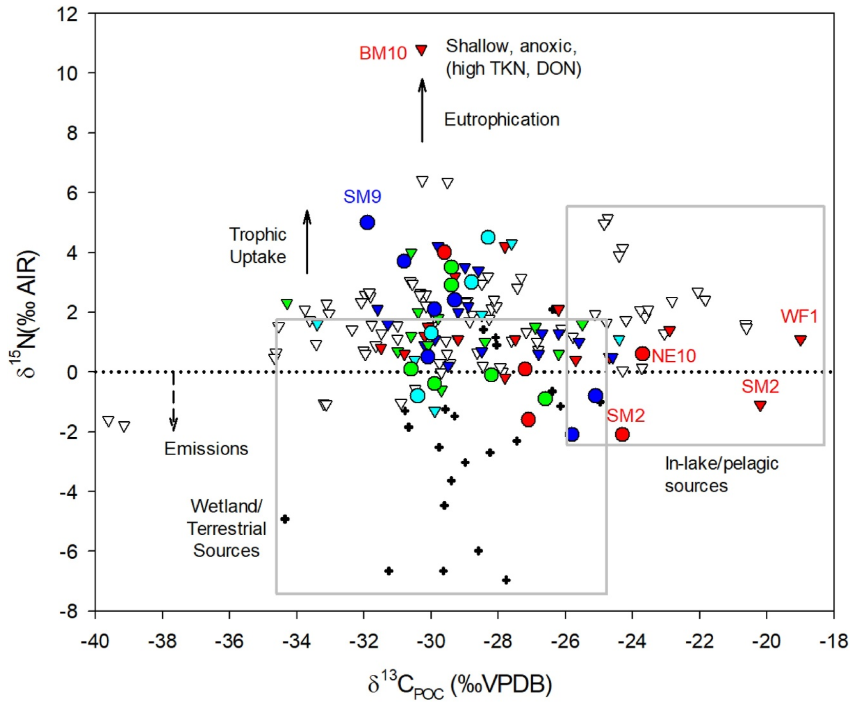

Figure 5. Nitrogen-15 and carbon-13 signatures in particulate organic matter sampled in RAMP Lakes in 2021 (colored triangles, $n = 50$) and RAMP Lakes 2022 (colored circles, $n = 40$). Thaw stages are defined based the classification of J. J. Gibson et al. (2019): 1-Rising Limb (blue; $n = 16$); 2-Falling Limb (cyan; $n = 5$); 3-Recession (green; $n = 10$); 4-Post thaw (red; $n = 9$). Results are compared to an unpublished 2009 survey of 125 lakes centered on the Stony Mountains (gray triangles) and a survey of wetland/terrestrial groundwater sources (black crosses) in the Stony Mountains and NE Ft McMurray by J. J. Gibson et al. (2021). Negative $\delta^{15}N$ appears typical of reducing conditions in groundwater whereas positive $\delta^{15}N$ is characteristic of oxidizing conditions in most water bodies. Arrows denote expected shifts in $\delta^{15}N$ due to emissions (Wieder et al., 2022), and trophic uptake/eutrophication (see Beaudoin et al., 2001). Box outlines are used to identify observed ranges in wetland/terrestrial groundwater sources and in-lake/pelagic sources, and are approximate Selected lakes with prominent eutrophication/trophic uptake or in-lake/pelagic sources are labeled by lake ID, most of which are post-thaw lakes.

somewhat extended ranges for both for $\delta^{13}C_{POC}$ and $\delta^{15}N_{POM}$. For better characterization of allochthonous sources, we also compared our lake data set to wetland/terrestrial surveys of groundwater from sites in the Stony Mountains and NE Ft. McMurray, where groundwater was sampled from surface to 8 m-depth in bogs, fens (poor to rich),and jack pine uplands, as a baseline prior to a nutrient amendment trial (Berryman et al., 2016; J. J. Gibson et al., 2021). By comparison, we find $\delta^{13}C_{POC}$ in the RAMP lakes to be largely consistent with the range reported for wetland/terrestrial sources (ranging from −34‰ to −25‰), with fewer occurrences of more enriched $\delta^{13}C$ values we infer to be significantly influenced by inorganic sources or by in-lake pelagic sources and recycling (−25‰ to −19 ‰VPDB) (Figure 5).

For $\delta^{15}N_{POM}$, wetland/terrestrial sources fall within the range of −8 to +2 ‰AIR, comparable to values reported by Wieder et al. (2022) for 10 plant species at six peatland sites in the region (−12‰ to +4‰AIR). In examining gradients in $\delta^{15}N_{POM}$ by distance from oil sands operations, Wieder et al. (2022) reported no conclusive proof of regional industrial influence, although surmised that emissions would be expected to contribute to more negative $\delta^{15}N$ values based on trends observed in some vegetation species. As compared to $\delta^{15}N_{POM}$ in wetland/terrestrial sources (Figure 5), the RAMP lakes show a range from −2 to +11 ‰AIR, comparable in many cases, but apparently fractionated and enriched by trophic uptake in about one-fourth of the population (see Beaudoin et al., 2001). Eutrophication, leading to extreme enrichment in $\delta^{15}N_{POM}$, appears to be occurring in a single RAMP lake (BM10; see Figure 5).

Overall, comparison with reference data confirms that carbon-nutrient conditions in RAMP lakes are fairly typical of regional lakes in general, and that attribution of RAMP $\delta^{13}C_{POC}$ signatures to allochthonous carbon-nutrient loads is supported by our available data sets. While inter-year differences for individual lakes were

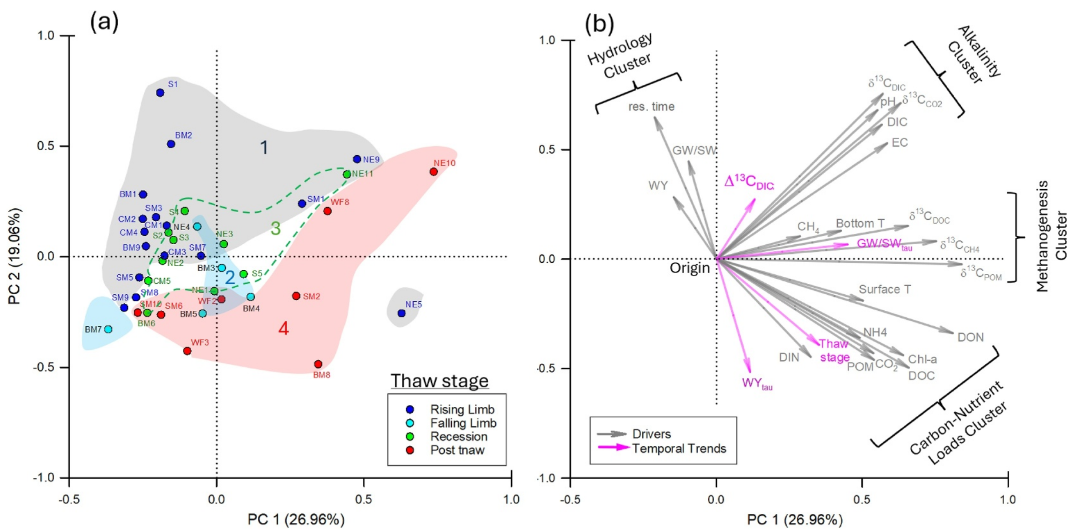

Figure 6. PCA plots showing (a) scores for individual lakes, grouped and color-coded by thaw stage (see legend), (b) major drivers of variability across the region considered in this analysis (gray vectors), and temporal trends based on Mann-Kendall tau scores (pink vectors). Clusters of driver types are identified, including: hydrology, alkalinity, carbon-nutrient loads, and methanogenesis. $\Delta^{13}C_{DIC}$ (pink vector) is also shown, based on differences between 2010 and mean values measured in 2020–2022. See text for discussion.

non-unidirectional and small (std. dev. = 1.6‰ for both tracers), maximum differences of up to 4.4 ‰ in $\delta^{13}C_{POC}$ and 2.9 ‰ in $\delta^{15}N_{POM}$ were found for individual lakes.

4.1.5. PCA Analysis of Site-Specific Drivers

A PCA analysis was conducted to examine and illustrate the significance of thaw-related impacts within the context of overall geochemical variations across the data set (Figure 6). A PCA score plot (Figure 6a) summarizes scores for individual lakes, while important drivers of variation across the data set are shown as vectors (Figure 6b). We note that lakes with average properties plot close the origin whereas lakes with distinctive characteristics are highlighted by degree of offset from the origin, as influenced by specific drivers. Four distinct clusters of drivers are evident, including those related to (a) alkalinity (EC, pH, DIC), (b) methanogenesis (CH_4), (c) carbon-nutrient loads (DON, DIN, POM, DOC, CO_2, Chl-a), and (d) hydrologic controls (WY, GW/SW, residence time). Note that the carbon isotope indicators, $\delta^{13}C_{DIC}$ and $\delta^{13}C_{CO2}$, cluster with the alkalinity drivers, owing to their dependence on DIC equilibria; $\delta^{13}C_{CH4}$ is coupled directly to methanogenesis and appears to be dependant the isotopic composition of organic substrates, $\delta^{13}C_{DOC}$ and $\delta^{13}C_{POC/POM}$. While no isotopic indicators were aligned directly with drivers of carbon-nutrient loads, we suggest that $\delta^{13}C_{DIC}$ and $\delta^{13}C_{CH4}$, and their combined influence on and $\delta^{13}C_{CO2}$ may be influential in labeling in-lake $\delta^{13}C_{DOC}$ and $\delta^{13}C_{POC}$ in pelagic sources, through DOC-DIC exchange and DOC sedimentation (see Figure 2).

Groups of lakes within each of four thaw stages proposed by J. J. Gibson et al. (2019) are also identified, showing representative ranges for each (Figure 6a). For groups 1 to 3, lakes with consequential permafrost in their watersheds (i.e., rising limb, falling limb, recession), variability occurs mainly along the PC2 axis, and is attributed primarily to hydrological factors, with individual scores falling mainly in the left quadrants of the PCA plots (Figure 6a). Exceptions include a few lakes (that plot in the right quadrants) which clearly differ from the majority owing to higher alkalinity (SM1, NE9, NE11) or higher carbon-nutrient loads (NE5, BM5). Variability among post-thaw lakes (Group 4) appears to be driven predominantly by water quality factors associated with PC1, although these also diverge in the right quadrants into subgroups affected more by alkalinity (WF8, NE10) and others affected more by carbon-nutrient loads (WF1, BM8, SM2). We point out that post-thaw lakes may be either hardwater (pH > 7.5), circumneutral (6.5 < pH < 7.5), or softwater lakes (pH < 6.5), or potentially eutrophic (BM10), factors which can lead to heterogeneity in the thaw succession response. Post-thaw lakes that do not become nutrient-rich or alkaline (and plot in the lower right quadrant), tend to have low carbonate alkalinity, commonly buffered by carboxylic acids (Castrillon-Munoz et al., 2022), they tend to be shallow, and have shorter

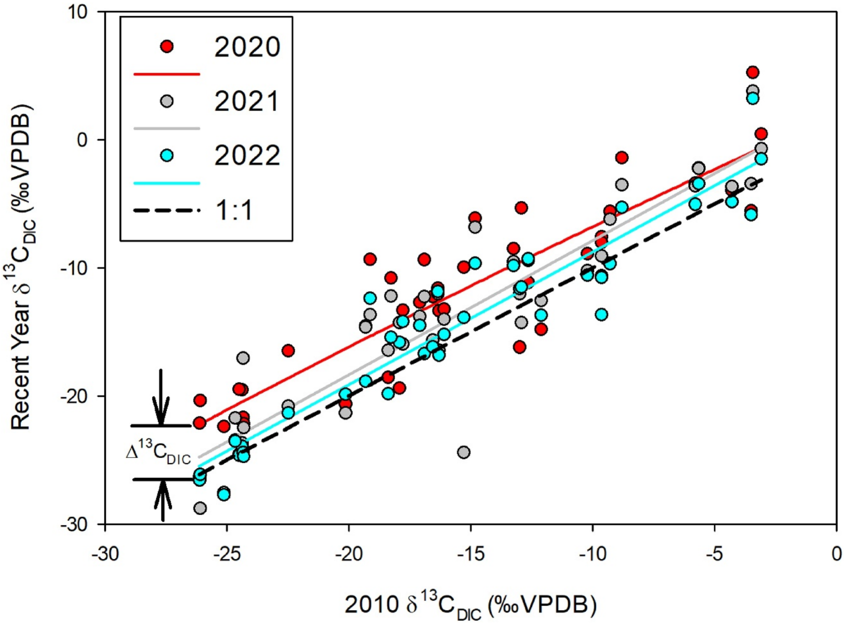

Figure 7. Crossplot of carbon-13 in dissolved inorganic carbon in RAMP lakes measured in 2010 compared with three recent sampling years (2020–2022). Shifts in $\delta^{13}C_{DIC}$ ($\Delta^{13}C_{DIC}$) are found to be positive for 2020–2022 years as compared to 2010, which is inferred to be due to systematic interannual changes in the carbon cycle balance in response to allochthonous carbon loading. Reversal in $\Delta^{13}C_{DIC}$ offset is noted for 2021 and 2022, after a record runoff year in 2020.

residence times, lower water yields (WY) and limited GW/SW interaction. Thaw status itself (pink vector, Figure 6b) is aligned clearly with carbon-nutrient loads, which indicates a strong influence of allochthonous loading in general along the permafrost thaw trajectory. $\Delta^{13}C_{DIC}$ is found to fall between alkalinity and hydrology drivers (Figure 6b), which is consistent with temporal adjustment in carbonate equilibria (and temperature, pH) as influenced by water flushing and allochthonous carbon loading, and potentially by methanogenesis.

Other trends shown on the PCA (Figure 6b) include WY_{tau}, which captures the general reduction in runoff as permafrost thaw sources are depleted, and GW/SW_{tau}, which signifies groundwater activation across the thaw gradient. Whereas WY and WY_{tau} are opposite to one another, suggesting that runoff and reduction in runoff are governed by similar controls found across the contemporary thaw trajectory, GW/SW and GW/SW_{tau} are mutually orthogonal, which suggests fundamental changes to groundwater controls in association with permafrost degradation. On first inspection, GW/SW_{tau} also appears to be aligned with methanogenesis drivers. We suggest that these processes are not necessarily coupled but coincident. Owing to accumulation of profundal sediments in the lake and apparent development of anoxic/methanogenic porewater conditions, these zones are not expected to support higher rates of groundwater discharge. However, enhanced groundwater inputs may be occurring along lake margins and within the littoral zone of lakes as perennial frozen ground is reduced. We postulate that this may occur concomitant with methanogenesis in deeper basinal areas of the lake, likely to be areas of higher carbon deposition. While Benoy et al. (2007) estimated that as much as 75% of allochthonous carbon storage is likely occurring in littoral zones, based on typical areal proportions for shallow lakes in boreal regions, carbon deposition in these zones may be important sources for oxic organic matter decomposition that may be influential in the overall carbon balance of lakes.

4.2. Thaw Trajectory Characterization

4.2.1. Landcover

Permafrost within the study region occurs in close association with permafrost-containing peat plateaus, and is generally correlated with percent area of bogs (Figure 8a) observed across the permafrost thaw gradient. Percent area of fens (Figure 8b), which have been described as forming and expanding as a result of bog collapse and succession (Vitt et al., 1994), are found to be anticorrelated with permafrost extent (Figure 8c), illustrating an inferred genetic relationship to bog collapse, and an indirect link to wetland forms with higher groundwater

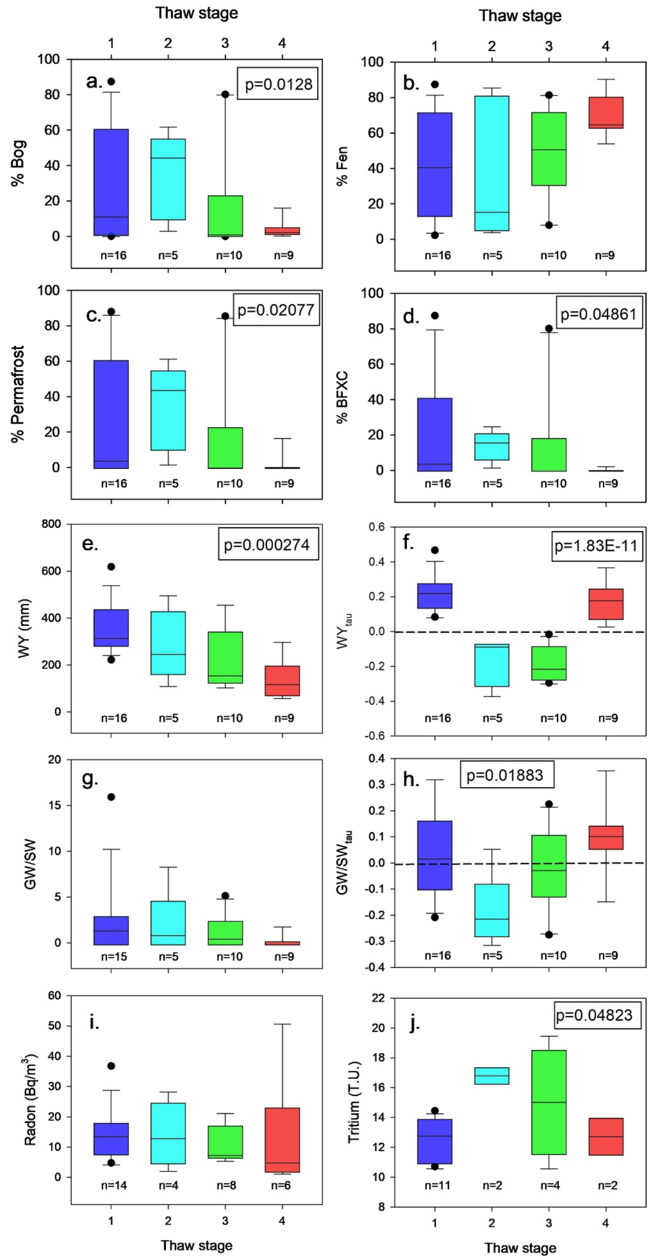

Figure 8. Box and whiskers plots showing variation in watershed characteristics and hydrologic response along the thaw trajectory (a) %Bog, (b) %Fen, (c) %Permafrost, and (d) %BFXC (Bog Forest Permafrost Collapse Scar), and isotope-based hydrologic indicators: (e) WY, (f) WYtau, (g) GW/SW, (h) GW/SWtau, (i) Radon-222, and (j) enriched tritium. Thaw stages are defined based the classification of J. J. Gibson et al. (2019): 1-Rising Limb (blue); 2-Falling Limb (cyan); 3-Recession (green); 4-Post thaw (red); n = number of lakes by category. Boxes denote 25th and 75th percentiles, whiskers denote 5th and 95th percentiles. Median values and outliers are also shown except one out-of-range value for GW/SW (see Table 2). Note that progression of land cover and hydrologic indicators is inferred to arise from wetland/permafrost succession. BFXC refers to bog areas displaying collapse scaring, which is direct evidence of permafrost thaw. Radon-222 is inferred to increase due to proportionate increase in groundwater flowpaths in contact with mineral soils versus peat, whereas tritium is inferred to be a proportionate indicator of permafrost-thaw contributions from recently formed (post-1950s) permafrost (see also J. J. Gibson et al., 2016). One-way ANOVA tests (Table S5 in Supporting Information S1) confirm distributions for %Bog, %permafrost, %BFXC, WY, WYtau, GW/SWtau, and enriched tritium are statistically significant ($p \leq 0.05$) among thaw stages; p-values for these variables are shown.

exchange potential (AESRD, 2015; Halsey et al., 2003). The occurrence, frequency and extent of bog forest permafrost collapse scar terrain (%BFXC, Figure 8d), bears a strong inverse relationship to our inferred hydrologic progression, and is significant as it is one of the few lines of direct evidence to support our hypothesis of permafrost-related succession across the study network (see also J. J. Gibson et al., 2015).

4.2.2. Hydrologic Indicators

Hydrological succession during permafrost thaw, previously described for the study lakes (J. J. Gibson et al., 2019, 2025), is characterized by systematic water yield (WY) decline (Figure 8e) whereas WY_{tau} (Figure 8f), the rate of change in WY calculated using the Mann-Kendall tau statistic, is shown to be periodic, decreasing from rising limb to falling limb and then increasing again in the recession and post thaw stages. Differences in the calculated GW/SW (Figure 8g) are also found to progress from the early thaw stages (1,2) where interaction is inferred to be relatively high due to presence of more intact permafrost, as compared to the latter stages (3,4) where a distinct reduction is noted. In comparison, GW/SW_{tau} (Figure 8h) closely mimics WY_{tau}, suggesting activation of shallow groundwater flowpaths to lakes during the rising limb, maximum rates of decline during the falling limb as permafrost is significantly reduced, and progressive increase in potential groundwater inputs along deeper flowpaths into the thaw recession and in the post-thaw stages. Radon-222 in lakewater (Figure 8i), which is included as an additional indicator of potential groundwater input to the lakes, appears to suggest that groundwater contributions may be active to varying degrees for lakes at all stages of the thaw progression. In general, radon levels are expected to be low in lakes fed by precipitation, surface runoff and/or shallow-seated groundwater sources, where flowpaths are confined within peat (e.g., suprapermafrost water), but presumably would be elevated in the case of lakes fed by contributions from deeper groundwater, along flowpaths that move through or in contact with surficial till and bedrock. Although no statistically significant differences were found among thaw stages, it does appear that radon levels range to higher values for some post-thaw lakes. Tritium, which is present in higher quantities in permafrost formed since the 1950s, has also been found to be elevated in lakes in the region receiving active thaw sources (J. J. Gibson et al., 2016). As shown (Figure 8j), enriched tritium content is significantly higher in study lakes within the falling limb and recession stages of the thaw trajectory. This is inferred to be a signal of permafrost thaw sources to lakes, although it is a partial signal, excluding older sources with low tritium which are undoubtedly present as well. Overall, the hydrologic progression we infer across the thaw trajectory is consistent with previous descriptions of hydrologic response in thawing permafrost systems.

Previous studies in lake-rich permafrost systems such as the Tibetan Plateau, northwestern Canada, and globally (Meredith et al., 2019) have suggested that continuous permafrost (and also extensive areal permafrost coverage), serves as an impermeable barrier to infiltration, enhancing lateral supra-permafrost groundwater flow, which likely contributes to increased WY. Early thawing in discontinuous-permafrost peatland terrain is commonly associated with enhanced runoff (Connon et al., 2014). As discontinuous permafrost degrades to 50% or so of areal coverage and becomes sporadic, water yields are often observed to decline both due to greater infiltration capacity in taliks, but also due to depletion of permafrost thaw sources (Wan et al., 2019). In the current setting, we postulate that sub-permafrost groundwater sources may also become more prevalent, influencing quantity and geochemical variability in runoff. Development of isolated discontinuous permafrost (coverage $<10\%$) has generally been found to result in further reduction in runoff as thaw sources continue to diminish, infiltration becomes more ubiquitous across the catchment, and groundwater pathways deepen and become more responsive to variations in the local hydrostratigraphy (Wan et al., 2019). In the post-thaw stage, where seasonal frozen ground dominates, precipitation-generated runoff and evaporation often become more influential, as does the character of the local hydrostratigraphy. It is important to note that the shallow depth of lakes (typically <4 m) tends to increase the influence of precipitation and surface runoff as input sources, although deeper connections can be important for individual lakes, particularly deeper lakes.

4.2.3. pH, DOC, DIC and POC

Within this hydrologic context we examined geochemical changes in lakes, which was one of the motivating factors to better understand permafrost thaw succession and its relation to widespread pH increase observed in the lakes (J. J. Gibson et al., 2025). pH is shown to be highly variable in lakes across the thaw trajectory (Figure 9a), however, pH_{tau} (Figure 9b) is found to be positive in most lakes within all thaw categories.

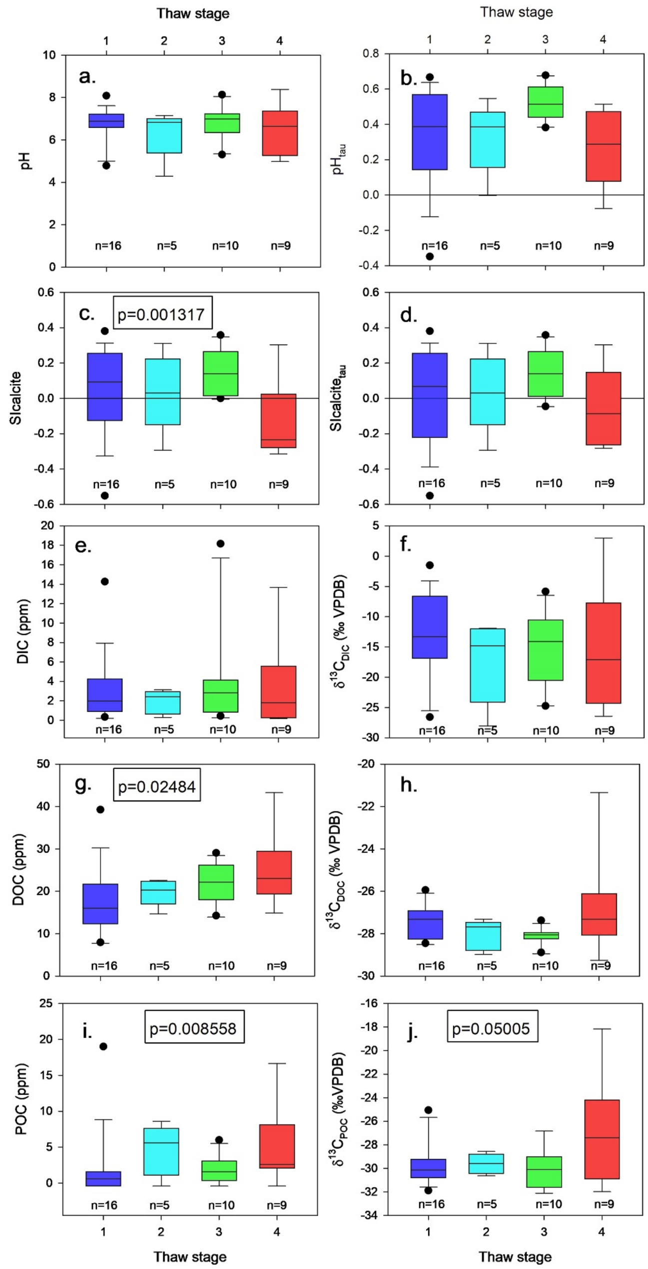

Figure 9. Box and whiskers plots showing selected thaw trajectory geochemical and isotopic characteristics (2002–2017) based on the classification of J. J. Gibson et al. (2019): (a) pH, (b) pH_{tau}, (c) SIcalcite, (d) $SIcalcite_{tau}$, (e) DIC, (f) $\delta^{13}C_{DIC}$, (g) DOC, (h) $\delta^{13}C_{DOC}$, (i) POC, and (j) $\delta^{13}C_{POC}$. Thaw stages are defined based the classification of J. J. Gibson et al. (2019): 1-Rising Limb (blue); 2-Falling Limb (cyan); 3-Recession (green); 4-Post thaw (red); n = number of lakes by category. Boxes denote 25th and 75th percentiles, whiskers denote 5th and 95th percentiles. Median values and outliers are also shown. While pH is variable among groups, pH_{tau} is predominantly positive. SIcalcite and $SIcalcite_{tau}$ suggest that supersaturated conditions (SI > 0) persist throughout stages 1–3, whereas post-thaw lakes (stage 4) commonly trend toward carbonate dissolution (SI < 0). Among individual carbon fractions, DOC and POC appear to show the most systematic increases across the thaw trajectory. ANOVA tests (Table S6 in Supporting Information S1) confirm distributions for SICalcite, POC, DOC and $\delta^{13}C_{POC}$ are significantly different ($p \leq 0.05$) among thaw stages; p-values for these variables are shown.

Based on a wide survey of geochemical parameters (Castrillon-Munoz et al., 2022; J. J. Gibson et al., 2025), this appears to be consistent with perturbations induced by introduction of allochthonous carbon sources, leading to alteration in resulting carbonate equilibria. Saturation with respect to calcite, $SI_{calcite}$ (Figure 9c) is found be to variable, but is maintained at near saturation levels overall, exhibiting typically positive values (precipitating) for lakes in stages 1–3 and negative values (dissolving) for post-thaw lakes (stage 4). Momentum in carbonate saturation, as indicated by $SIcalcite_{tau}$ (Figure 9d) suggests positive tendencies for lakes within stages 1–3 and a negative tendency for post-thaw lakes (stage 4), which preliminarily, we considered a reasonable indicator of carbon loading intensity. Differences between dilute, softwater lakes, dominated by carboxylic acid buffering, and hardwater lakes buffered by carbonate alkalinity explains much of the variability in pH and $SI_{calcite}$ observed within individual thaw stages (see Castrillon-Munoz et al., 2022).

Variations in the carbon fractions, DIC, DOC and POC, as well as their isotopic signatures (Figures 9e–9j) also reveal characteristic patterns. Notably, we found that lakes had significant DOC and POC differences among the thaw stages, with very systematic progression to higher DOC concentrations in successive thaw stages (Figure 9g), accompanied by a less-regular progression in POC (Figure 9i). DIC concentrations do not appear to show any significant differences across the thaw stages, which may reflect the overriding dependence of DIC on regulation by in-lake carbonate equilibria, which may also be potentially masking the effect of DIC inputs. On examination of the isotopic signatures of DIC, DOC, and POC, we note a significant reduction in median $\delta^{13}C_{DIC}$ (Figure 9f) and increase in median $\delta^{13}C_{DOC}$ and $\delta^{13}C_{POC}$ (Figures 9h and 9j) in post-thaw lakes (stage 4), although again with apparently high lake-to-lake variability.

By comparison with the hydrologic indicators, we also observe apparently strong inverse coupling between in DOC (Figure 9g) with WY (Figure 8e), and direct coupling between $\delta^{13}C_{DOC}$ (Figure 9h) with WYtau and GW/SWtau (Figures 8f and 8h) across the entire thaw trajectory.

Considering the progression in both water fluxes and DOC and POC concentrations, it is apparent that peak allochthonous carbon loads are likely occurring during the falling limb and recession stages of permafrost thaw (stages 2 and 3), similar to the progression found in tritium (Figure 8j), and associated with a reduced, depleted range in $\delta^{13}C_{DOC}$ values (Figure 9h). We note that the range of $\delta^{13}C_{DOC}$ and $\delta^{13}C_{POC}$ in lakes is also similar in most cases to wetland/terrestrial sources as measured in our separate watershed surveys (Figure 5).

Overall, we attribute allochthonous carbon loading during active permafrost thaw to play a dominant role contributing to increase in carbonate saturation, that we infer is likely the result of biogenic degradation and respiration of DOC and POC, which enhances in-lake CO_2. During post-thaw, as allochthonous carbon inputs are reduced, carbonate saturation appears to be controlled predominantly by in-lake processes such as pelagic uptake, methanogenesis, or local factors such as presence or absence of carbonate rocks.

The main interactions we have described are reasonably consistent with our conceptual model (Figure 2), which integrates our observations from the RAMP investigations as well as numerous other studies carried out in northern regions with degrading permafrost. In general, such studies have shown permafrost degradation to be associated in most cases with increased allochthonous carbon loading to lakes (Turetsky et al., 2019). Apart from limited prior opportunities (J. J. Gibson et al., 2015), constraints of the field program have not permitted regular sampling of watershed runoff sources, so our interpretation has necessarily been restricted to inferences based on lakewater sampling, although these are considered fairly reliable for assessing carbon cycle sources.

4.2.4. Dissolved CO_2 and CH_4

While dissolved CO_2 is found to increase across the thaw gradient (Figure 10a), generally in lock-step with DOC (Figure 9e), its isotopic signature, $\delta^{13}C_{CO2}$ (Figure 10b) shows a similar periodicity as found for $\delta^{13}C_{DOC}$ (Figure 9h) and the hydrologic trend indicators, WYtau and GW/SWtau (Figures 8f and 8h). We also attribute this progression to the effect of allochthonous loading on both CO_2 concentration and its isotopic signature, which accounts for increasing DOC concentrations as well as hydrologic flushing. For comparison, we include CO_2 levels and $\delta^{13}C_{CO2}$ predicted based on carbonate equilibrium with the atmosphere (red cross hatches, Figures 10a and 10b), which suggests in the case of the RAMP lakes that CO_2 supersaturation is driven by carbon loading, that it is sustained throughout the stages of thaw, but that $\delta^{13}C_{CO2}$ is controlled also by rates of hydrologic flushing as well as atmospheric exchange. By contrast, CH_4 concentrations are found to show no clear trends during thaw progression (Figure 10c), although $\delta^{13}C_{CH4}$ displays a similar pattern to that of $\delta^{13}C_{CO2}$ (Figure 10d) reflecting a detectable flushing control. As described previously in reference to Figure 4, enrichment in $\delta^{13}C_{CH4}$ tends to be most prevalent in post thaw lakes, which is also revealed in Figure 10d. Overall, we posit that methanogenesis by acetate fermentation driven by allochthonous carbon loading is likely occurring throughout the thaw process in most lakes, but that methane oxidation may be more prevalent during the post-thaw stages, which contributes to

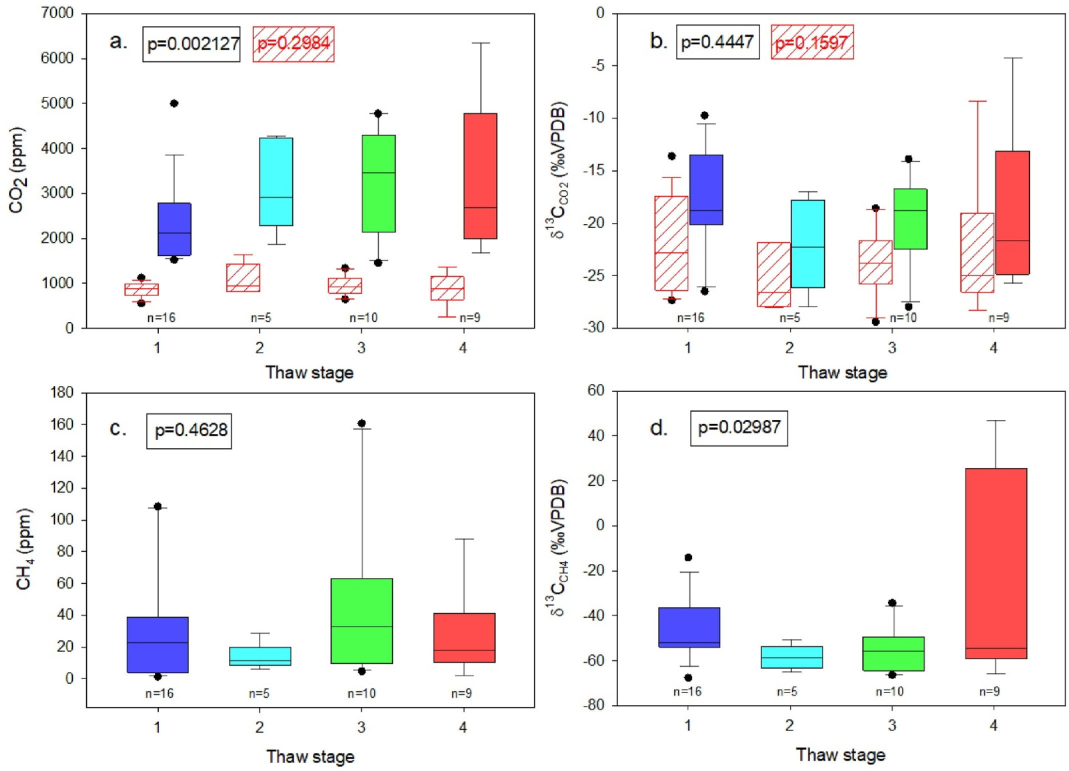

Figure 10. Box and whiskers plots showing gas concentrations and distribution of carbon-13 values for CO_2 and methane in lakes situated across the observed permafrost thaw gradient. Thaw stages are defined based the classification of J. J. Gibson et al. (2019): 1-Rising Limb (blue); 2-Falling Limb (cyan); 3-Recession (green); 4-Post thaw (red); n = number of lakes by category. Boxes denote 25th and 75th percentiles, whiskers denote 5th and 95th percentiles. Median values and outliers are also shown. Red cross-hatching for (a) CO_2 and (b) $\delta^{13}C_{CO2}$ illustrate reference values calculated assuming CO_2 sources in DIC equilibrium with the atmosphere. Higher ranges found for CO_2 and $\delta^{13}C_{CO2}$ than accounted for by DIC equilibrium are attributed to influence of additional carbon sources (i.e., allochthonous carbon, groundwater, methanogenesis). CO_2 concentrations were found to increase systematically across the thaw gradient whereas distribution of CH_4 and $\delta^{13}C_{CH4}$ is less regular. Prevalence of methane oxidation largely explains increased $\delta^{13}C_{CH4}$ values for post-thaw lakes. ANOVA tests (Table S7 in Supporting Information S1) confirm distributions for CO_2 and $\delta^{13}C_{CH4}$ are significantly different among thaw stages ($p \leq 0.05$); p-values for all variables are shown. (c) Methane concentration in lake water, and (d) $\delta^{13}C$ of dissolved methane in lakewater.

accelerated isotopic enrichment of methane. Very high CH_4 concentrations were also measured in some recession lakes, which may be attributed to higher generation rates and lower rates of methane oxidation in this thaw stage where permafrost becomes sporadic but is not yet absent, and allochthonous carbon imports are still active. High CH_4 and less enriched $\delta^{13}C_{CH4}$ appears to be characteristic of many recession lakes and may potentially be a useful differentiator of lakes with residual permafrost and those without.

4.2.5. $\Delta^{13}C_{DIC}$ as a Temporal Indicator

Previous studies have applied $\delta^{13}C_{DIC}$ in surface waters and groundwaters to infer the balance between inorganic versus organic carbon sources, as well as to identify regional shifts in this balance (Campeau et al., 2017; Helie & Hillaire-Marcel, 2006). Such assessments are enabled by natural labeling of $\delta^{13}C_{DIC}$, which acquires a distinctive signature dependent on its source. For example, DIC derived from inorganic weathering sources often falls within −5 to +5‰ ‰VPDB, the range found in marine carbonate rocks (Saltzman & Thomas, 2012), as compared to sources associated with allochthonous carbon import, also an important carbon source for autotrophic respiration, which align with the local signature of C3 plants (∼−27 to −28 ‰ VPDB; Kohn, 2010, eq. 1), as modified by dissolution and atmosphere exchange in soilwater solution, which typically can lead to 1–4‰ enrichment (Campeau et al., 2017).

Lake metabolism, including respiration and primary production, appear to be less influential in regulation of DIC and $\delta^{13}C_{DIC}$ than carbonate dissolution for the RAMP lakes, based on the criteria described by de Kluijver et al. (2014), as previously noted. Geochemical modeling has also confirmed that the lakes are generally supersaturated with respect to CO_2 (Castrillon-Munoz et al., 2022). While supersaturation has the potential to enhance primary productivity (Jansson et al., 2012), this effect is currently limited to a small number of post-thaw lakes with apparent $\delta^{13}C_{DIC}$ enrichment (see Figure 5). Supersaturation may also promote CO_2 evasion, but can also serve to limit back exchange of atmospheric CO_2 (Benoy et al., 2007). Based on our observations we suggest that the RAMP Lakes are potential sources of carbon to the atmosphere in the form of both CO_2 and CH_4, but assessment of the extent to which allochthonous organic carbon may be buried and sequestered in lake sediments (Pace & Prairie, 2005) remains to be investigated.

One approach that we set out to specifically test is whether $\Delta^{13}C_{DIC}$ (Figure 8) may be a useful indicator of thaw trajectory evolution, and if so, do we see incremental progression in $\Delta^{13}C_{DIC}$ in interannual data collected between 2010 and 2022. Here we define $\Delta^{13}C_{DIC}$ as the difference between $\delta^{13}C_{DIC}$ measured in a recent year (i.e., 2020, 2021 or 2022) versus $\delta^{13}C_{DIC}$ measured in 2010. As such, increases in $\delta^{13}C_{DIC}$ in a lake over a time interval correspond to positive values of $\Delta^{13}C_{DIC}$, analogous to $\delta^{13}CDIC_{tau}$ but relying on discrete measurements rather than trends in continuous observations over time.

$\Delta^{13}C_{DIC}$ was shown by J. J. Gibson et al. (2025) to systematically increase during the interval between 2010 and 2020, which appears to have resulted from adjustment in carbonate equilibria propelled by allochthonous carbon loading, which also expected to depend not only on carbon concentration of input but also on the volume of water input from the watershed (i.e., a dilution effect). When we compared $\Delta^{13}C_{DIC}$ between recent years (2020, 2021, 2022) and 2010 (Figure 7), this offset was found to become progressively reduced in 2021 and 2022. It is important to note that $\Delta^{13}C_{DIC}$ values are an order of magnitude greater than analytical uncertainty and are distinct from patterns noted for $\delta^{13}C_{DIC}$ itself. Given that 2022 was a record-high runoff year across the region, our conclusion is that $\Delta^{13}C_{DIC}$ may be increasing/decreasing interannually due to variations in rates of flushing and resulting dilution of allochthonous carbon imports.

We also tested whether $\Delta^{13}C_{DIC}$ may be a useful indicator in our thaw trajectory assessment by comparing average $\delta^{13}C_{DIC}$ in 2020–2022 to that measured in 2010 (Figure S1 in Supporting Information S1), and observed a familiar pattern of periodic change across the permafrost thaw trajectory. Similar responses were noted for all subcategories of lakes including softwater, circumneutral, and hardwater lakes, as well as lakes with and without methane oxidation (Figure S1 in Supporting Information S1). Overall, we conclude that $\Delta^{13}C_{DIC}$ (and $\delta^{13}C_{DIC}$) is responding mainly to allochthonous carbon loading and may be a useful overall indicator of this process for both site-specific and thaw-trajectory based characterization.

5. Carbon Cycle Processes and Permafrost Thaw

Systematic carbon cycle changes have accompanied permafrost thaw, which has been widespread across northeastern Alberta for about 150 years and has likely accelerated due to anthropogenic causes over the last few decades. We have applied a "permafrost thaw trajectory" approach as a space-for-time analog to describe the likely succession of related impacts to the hydrological and geochemical cycles, and have described or inferred carbon cycle interactions that are currently underway across the permafrost thaw trajectory. Such changes can be viewed as part of the systematic succession of peatlands and permafrost landscapes across the boreal forest regions of northeastern Alberta and western Canada. As noted in many paleolimnological investigations, and observed from our studies relying on RAMP, lakes are key nodes in the regional drainage network and provide important historical records useful for study of environmental change. Because lakes are receiving water bodies for larger areas of the surrounding landscape, environmental signals are often spatially representative of larger areas, and due to the water residency effect, they are temporally representative of longer time periods. In the present setting, which is wetland-dominated, the combination of landscape position and weighting effects appears to render useful signals which capture long-term (inter-decadal) evolution of permafrost thaw impacts. As a result, lakes at different stages across the thaw trajectory are found to follow distinct patterns of hydrologic progression analogous to a space-for-time hydrograph and described using similar terminology (i.e., rising limb, falling limb, recession, post thaw, see J. J. Gibson et al., 2019, 2025). Our observations also support the concept of hydrological response units, with landscape-dependent and connectivity-dependent controls, as described in numerous studies in the western boreal forest region (Connon et al., 2014; Devito et al., 2005, 2017; Eum et al., 2017; Quinton et al., 2009; Smerdon et al., 2005).

Castrillon-Munoz et al. (2022) showed that pH increase in the lakes is regulated by two main geochemical processes, namely, carbonate dissolution and organic matter uptake (i.e., decomposition to form CO_2). Lakes in many subregions showed evidence of dissolution of marine carbonates, likely derived from surficial till and/or bedrock. From geochemical modeling, lake water was predicted to be CO_2 super-saturated, which we have confirmed based on dissolved gas measurements. A progression in $\delta^{13}C_{DIC}$ also confirms systematic evolution in the carbon cycle balance in lakes across the thaw gradient. These findings, combined with direct evidence of $\delta^{13}C$ and $\delta^{15}N$ values consistent with terrestrial and wetland sources, supports the general hypothesis that allochthonous loading is the main agent of carbon cycle changes occurring across the thaw trajectory.

Evidence of water sources and flowpath depths from enriched tritium and radon-222 are also shown to be mechanistically informative. Tritium levels in lakes mimic hydrologic trends observed in WY_{tau} and GW/SW_{tau}, that are attributed to increase in runoff due to the release and subsequent recession of thaw sources with higher tritium. We infer this water to be associated with permafrost thaw from sources formed in the post-1950 period. Variable radon-222 content, which is acquired by water-rock interaction with till or bedrock, suggests that flowpath depths may vary widely among lakes, but higher and more variable radon-222 in post-thaw lakes appears to point to development of deeper flow systems in general.

Our analysis also confirms the role of acetoclastic methanogenesis and methane oxidation as sinks or recycling pathways for carbon, which may be influential regulatory controls on CO_2 and carbonate equilibria in the lakes. Overall, these observations have contributed to a better conceptual understanding of carbon storages and interactions in RAMP lakes, and their susceptibility to permafrost thaw (Figure 2). Further work is needed to quantify the net effect of permafrost thaw on overall regulation of carbon sources and sinks across the region. Our study has identified several important control variables that can be straightforwardly incorporated into routine water quality monitoring, such as $\delta^{13}C_{DIC}$, $\delta^{13}C_{DOC}$, and $\delta^{13}C_{POC}$, that can be applied to monitor and predict carbon cycle evolution in the lakes. We have identified that classification of the thaw stage, geochemical drivers, and hydrogeologic context is helpful to understanding site-specific responses to climate change and for prediction in what otherwise appears to be a disorganized and heterogeneous landscape.

6. Limitations

The principal limitation of this study is that isotopic characterization of the carbon cycle components was mainly carried out in 1 year. Confirmation of similar $\delta^{13}C_{DIC}$ patterns in 2010, 2020, 2021, and 2022 allowed us to establish that lake-to-lake variability was not being radically altered despite interannual differences, although regular annual monitoring would have been an improvement. Our study focused on examining regional survey data in the context of spatial variations associated with the thaw trajectory. However, depth-wise and seasonal sampling (including under ice) was not conducted, but would be required to develop a more quantitative description of carbon cycling processes. Detailed process studies at an individual site or sites should ideally include an examination of hydrochemical evolution in bog and fen collapse scars adjacent to the lake, and investigation of in-lake controls on methanogenesis and atmospheric CO_2 exchange as important greenhouse gas sources.

One fundamental limitation of the RAMP lakes program in general is that it has been paused since 2022 (and may potentially be discontinued) as new monitoring strategies are being evaluated by the Joint Oil Sands Monitoring Program. Our research suggests that the original goal of lake acidification monitoring will require longer-term monitoring to assess site-specific impacts as these effects may be currently masked by enhanced water and carbon loading in many lakes owing to permafrost thaw. Given that the RAMP lakes are a fair representation of typical systems across the region, which our investigations suggest, continuity in monitoring is likely more important than pre-selection of sites with specific or distinctive features. Within the context of the RAMP lakes, it is possible that lakes in the post-thaw phases might be better analogs or early warning indictors for acidification, which serves the original purpose of the RAMP lakes network, although comparison across the thaw trajectory remains informative as well.

7. Conclusions

Surveys of representative lakes situated across a permafrost thaw gradient in northeastern Alberta have provided new insights into carbon cycle processes, mechanisms of change, and their anticipated trajectories. New measurements of stable isotope composition of various carbon reservoirs across a thaw trajectory assisted in quantifying these processes, including the significant impact of carbon release from surrounding peatlands. While site-specific conditions are heterogeneous and complex, environmental responses are more systematic and predictable when viewed in the context of the permafrost trajectory, which reveals non-monotonic responses for runoff, groundwater and allochthonous carbon release. The main effects of permafrost thaw on lakes in the region that we were able to establish include: periodic hydrologic flushing of lakes by significant thawing of permafrost, destabilization of established peatlands that contribute to allochthonous loading of organic carbon stores from the watershed, enhancement of biogenic CO_2 in lakes which increases carbonate saturation, and acceleration of acetoclastic methanogenesis and methane oxidation, the latter becoming potentially more prevalent during the post-thaw stages. We suggest that a similar stratified, thaw-trajectory approach may be suitable for characterization of carbon cycle changes in lake-rich regions across the boreal forest and arctic which are currently undergoing accelerated permafrost degradation.

Conflict of Interest

The authors declare no conflicts of interest relevant to this study.

Data Availability Statement

Data are downloadable in excel format at: https://zenodo.org/records/18135830. Supporting data sets are described in an open access Data in Brief article (J. J. Gibson et al., 2020) available at: https://doi.org/10.1016/j.dib.2020.105308.

Acknowledgments

We thank OSM and AEPA for supporting incorporation of our sampling requirements within the existing field program, as well as access to monitoring data. We also gratefully acknowledge financial support from InnoTech Alberta, Canada and the Natural Sciences and Engineering Research Council Canada which assisted isotopic and geochemical analysis. Historical support from RAMP, Wood Buffalo Environmental Association, and the Cumulative Environmental Management Association was also essential to our research.

References

Aherne, J., & Shaw, D. P. (2010). Impacts of sulphur and nitrogen deposition in western Canada. *Journal of Limnology*, *69*(1S), 1–3. https://doi.org/10.4081/jlimnol.2010.s1.1

Alberta Environment. (2002). *Water quality sampling methods*. Water Monitoring Group, Compliance Branch, Regional Services, Alberta Environment.

Alberta Environment. (2006). Aquatic ecosystems field sampling protocols. Retrieved from https://open.alberta.ca/publications/077855080x

Alberta Environment and Sustainable Resource Development. (2015). *Alberta wetland classification system* (p. 66). Water Policy Branch, Policy and Planning Division.

Arnoux, M., Barbecot, F., Gibert-Brunet, E., Gibson, J., & Noret, A. (2017). Impacts of changes in groundwater recharge on the isotopic composition and geochemistry of seasonally ice-covered lakes: Insights for sustainable management. *Hydrology and Earth System Sciences*, *21*(11), 5875–5889. https://doi.org/10.5194/hess-21-5875-2017

Assayag, N., Rive, K., Ader, M., Jezequel, D., & Agrinier, P. (2006). Improved method for isotopic quantitative analysis of dissolved inorganic carbon in natural water samples. *Rapid Communications in Mass Spectrometry*, *20*(15), 2243–2251. https://doi.org/10.1002/rcm.2585

Beaudoin, C. P., Prepas, E. E., Tonn, W. M., Wassenaar, L. I., & Kotak, B. G. (2001). A stable carbon and nitrogen isotope study of lake food webs in Canada's Boreal Plain. *Freshwater Biology*, *46*(4), 465–477. https://doi.org/10.1046/j.1365-2427.2001.00688.x

Beilman, D. W., Vitt, D. H., & Halsey, L. A. (2000). Localized permafrost peatlands in western Canada: Definition, distributions, and degradation. *Arctic Antarctic and Alpine Research*, *33*(1), 70–77. https://doi.org/10.1080/15230430.2001.12003406

Bennett, K. E., Gibson, J. J., & McEachern, P. (2008). Water yield estimates for critical loadings assessment: Comparisons of gauging methods vs. an isotopic approach. *Canadian Journal of Fisheries and Aquatic Sciences*, *65*, 83–99. https://doi.org/10.1139/7-155

Bennett, K. E., Schwenk, J., Bachand, C., Gasarch, E., Stachelek, J., Bolton, W. R., & Rowland, J. C. (2023). Recent streamflow trends across permafrost basins of North America. *Frontiers in Water*, *5*, 1099660. https://doi.org/10.3389/frwa.2023.1099660

Benoy, G., Cash, K., McCauley, E., & Wrona, F. (2007). Carbon dynamics in lakes of the boreal forest under a changing climate. *Environmental Reviews*, *15*(NA), 175–189. https://doi.org/10.1139/A07-006

Berryman, S., Birks, S. J., Gibson, J. J., Straker, J., Vile, M., Vitt, D., et al. (2016). Nitrogen critical loads five-year final report: Bog, poor fen, and jack-pine ecosystems. Technical report prepared for Cumulative Environmental Management Association (p. 201).

Biskaborn, B. K., Smith, S. L., Noetzli, J., Matthes, H., Vieria, G., Streletskiy, D. A., et al. (2019). Permafrost is warming at a global scale. *Nature Communications*, *10*(1), 264. https://doi.org/10.1038/s41467-018-08240-4

Blois, J. L., Williams, J. W., Fitzpatrick, M. C., Jackson, S. T., & Ferrier, S. (2013). Space can substitute for time in predicting climate-change effects on biodiversity. *Proceedings of the National Academy of Sciences*, *110*(23), 9374–9379. https://doi.org/10.1073/pnas.1220228110

Campeau, A., Wallin, M. B., Giesler, R., Lofgren, A., Morth, C.-M., Schiff, S., et al. (2017). Multiple sources and sinks of dissolved inorganic carbon across Swedish streams, refocusing the lens of stable C isotopes. *Nature*, *7*(1), 9158. https://doi.org/10.1038/s41598-017-09049-9

Castrillon-Munoz, F. J., Gibson, J. J., & Birks, S. J. (2022). Carbon dissolution effects on pH changes of RAMP lakes in northeastern Alberta, Canada. *Journal of Hydrology: Regional Studies*, *40*, 101045. https://doi.org/10.1016/j.ejrh.2022.101045

Connon, R. F., Quinton, W. L., Craig, J. R., & Hayashi, M. (2014). Changing hydrologic connectivity due to permafrost thaw in the lower Liard River valley, NWT, Canada. *Hydrological Processes*, *28*(14), 4163–4176. https://doi.org/10.1002/hyp.10206

Curtis, C. J., Flower, R., Rose, N., Shilland, J., Simpson, G. L., Turner, S., et al. (2010). Palaeolimnological assessment of lake acidification and environmental change in the Athabasca Oil Sands Region, Alberta. *Journal of Limnology*, *69*(S1), 92–104. https://doi.org/10.4081/jlimnol.2010.s1.92

De Kluijver, A., Schoon, P. I., Downing, J. A., Schouten, S., & Middelburg, J. J. (2014). Stable carbon isotope biogeochemistry of lakes along a trophic gradient. *Biogeosciences*, *11*(22), 6265–6276. https://doi.org/10.5194/bg-11-6265-2014

Denfeld, B. A., Lupon, A., Sponseller, R. A., Laudon, H., & Karlsson, J. (2020). Heterogeneous CO_2 and CH_4 patterns across space and time in a small boreal lake. *Inland Waters*, *10*(3), 348–359. https://doi.org/10.1080/20442041.2020.1787765

Devito, K., Creed, I., Gan, T., Mendoza, C., Petrone, R., Silins, U., & Smerdon, B. (2005). A framework for broad-scale classification of hydrologic response units on the Boreal Plain: Is topography the last thing to consider? -Invited Review. *Hydrological Processes*, *19*(8), 1705–1714. https://doi.org/10.1002/hyp.5881

Devito, K. J., Hokanson, K. J., Moore, P. A., Kettridge, N., Anderson, A. E., Chasmer, L., et al. (2017). Landscape controls on long-term runoff in subhumid heterogeneous Boreal Plains catchments. *Hydrological Processes*, *31*(15), 2737–2751. https://doi.org/10.1002/hyp.11213

Durridge (2025). Big bottle system manual. https://durridge.com/products/big-bottle-system/

Eum, H.-I., Dibike, Y., & Prowse, T. (2017). Climate-induced alteration of hydrologic indicators in the Athabasca River Basin, Alberta, Canada. *Journal of Hydrology*, *544*, 327–342. https://doi.org/10.1016/j.jhydrol.2016.11.034

Feng, D., Gleason, C. J., Lin, P., Yang, X., Pan, M., & Ishitsuka, Y. (2021). Recent changes to Arctic river discharge. *Nature Communications*, *12*(1), 6917. https://doi.org/10.1038/s41467-021-27228-1

Finlay, K., Vogt, R., Bogard, M., Wissel, B., Tutolo, B. M., Simpson, G. L., & Leavitt, P. R. (2015). Decrease in CO_2 efflux from northern hardwater lakes with increasing atmospheric warming. *Nature*, *519*(7542), 215–218. https://doi.org/10.1038/nature14172

Gibson, C. M., Chasmer, L. E., Thompson, D. K., Quinton, W. L., Flannigan, M. K., & Oldefeldt, D. (2018). Wildfire as a major driver of recent permafrost thaw in boreal peatlands. *Nature Communications*, *9*(1), 3041. https://doi.org/10.1038/s41467-018-05457-1

Gibson, J. J., Birks, S. J., McEachern, P., Hazewinkel, R., & Kumar, S. (2010). Interannual variations in water yield to lakes in northeastern Alberta: Implications for estimating critical loads of acidity. *Journal of Limnology*, *69*(Suppl. 1), 126–134. https://doi.org/10.4081/jlimnol.2010.s1.126

Gibson, J. J., Birks, S. J., & Yi, Y. (2016). Higher tritium concentrations measured in permafrost thaw lakes, northern Alberta. *Hydrological Processes*, *30*(2), 245–249. https://doi.org/10.1002/hyp.10599

Gibson, J. J., Birks, S. J., Yi, Y., Moncur, M. C., Vallarino, A., Kusel, C., et al. (2021). Hydrology and geochemistry studies in the oil sands region to investigate the role of terrain conductivity in nitrogen critical loads. *Water*, *13*(16), 2204. https://doi.org/10.3390/w13162204

Gibson, J. J., Birks, S. J., Yi, Y., & Vitt, D. (2015). Runoff to boreal lakes linked to land cover, watershed morphology and permafrost melt: A 9-year isotope mass balance assessment. *Hydrological Processes*, *29*(18), 3848–3861. https://doi.org/10.1002/hyp.10502

Gibson, J. J., Eby, P., Birks, S. J., Twitchell, C., Gray, C., & Kariyeva, J. (2022). Isotope-based water balance assessment for open water wetlands across Alberta: Regional trends with emphasis on oil sands regions. *Journal of Hydrology Regional Studies*, *40*, 101036. https://doi.org/10.1016/j.ejrh.2022.101036

Gibson, J. J., Jaggi, A., & Castrillon-Munoz, F. J. (2025). Widespread pH increase and geochemical trends in fifty boreal lakes: Evidence, prediction and plausible attribution to climate and permafrost thaw impacts across northeastern Alberta. *Journal of Hydrology Regional Studies*, *58*, 102253. https://doi.org/10.1016/j.ejrh.2025.102253

Gibson, J. J., & Peters, D. L. (2022). Water and environmental management in oil sands regions. *Journal of Hydrology: Regional Studies*, *44*, 101274. https://doi.org/10.1016/j.ejrh.2022.101274

Gibson, J. J., Yi, Y., & Birks, S. J. (2019). Isotopic tracing of hydrologic drivers including permafrost thaw status for lakes across northeastern Alberta, Canada: A 16-year, 50-lake perspective. *Journal of Hydrology: Regional Studies*, *26*, 100643. https://doi.org/10.1016/j.ejrh.2019.100643

Gibson, J. J., Yi, Y., & Birks, S. J. (2020). Watershed, climate, and stable isotope data (oxygen-18 and deuterium) for 50 boreal lakes in the oil sands region, northeastern Alberta, Canada, 2002–2017. *Data in Brief*, *29*, 105308. https://doi.org/10.1016/j.dib.2020.105308

Graven, H., Keeling, R. F., & Rogelj, J. (2020). Changes to carbon isotopes in atmospheric CO_2 over the industrial era and into the future. *Global Biogeochemical Cycles*, *34*(11), e2019GB006170. https://doi.org/10.1029/2019GB006170

Halsey, L. A., Vitt, D. H., Beilman, D., Crow, S., Mehelcic, S., & Wells, R. (2003). *Alberta wetlands inventory standards version 2.0. Alberta sustainable development* (pp. 1–54). Resource Data Branch, Strategic Corporate Services Division, Alberta Sustainable Resource Development.

Hatfield Consultants. (2016). Regional aquatics monitoring program in support of the joint oil sands monitoring plan. 2015 Final Program Report prepared for Alberta Environmental Monitoring, Evaluation and Reporting Agency (p. 1272).

Heffernan, L., Jassey, V. E. J., Frederickson, M., MacKenzie, M. D., & Olefeldt, D. (2021). Constraints on potential enzyme activities in thermokarst bogs: Implications for the carbon balance of peatlands following thaw. *Global Change Biology*, *27*(19), 4711–4726. https://doi.org/10.1111/gcb.15758

Helie, J. F., & Hillaire-Marcel, C. (2006). Sources of particulate and dissolved organic carbon in the St. Lawrence River: Isotopic approach. *Hydrological Processes*, *20*(9), 1945–1959. https://doi.org/10.1002/hyp.5962

Holmes, M. E., Chanton, J. P., Tfaily, M. M., & Ogram, A. (2015). CO_2 and CH_4 isotope compositions and production pathways in a tropical peatland. *Global Biogeochemical Cycles*, *29*, 1–18. https://doi.org/10.1002/2014GB004951

Holmes, R. M., Coe, M. T., Fiske, G. J., Gurtovaya, T., McClelland, J. W., Shiklomanov, A. I., et al. (2013). Climate change impacts on the hydrology and biogeochemistry of Arctic rivers. In *Climatic change and global warming of inland waters* (pp. 1–26). https://doi.org/10.1002/9781118470596.ch1

Holmes, R. M., McClelland, J. W., Raymond, P. A., Frazer, B. B., Peterson, B. J., & Stieglitz, M. (2008). Lability of DOC transported by Alaskan rivers to the Arctic Ocean. *Geophysical Research Letters*, *35*(3), L03402. https://doi.org/10.1029/2007GL032837

in't Zandt, M. H., Liebner, S., & Welte, C. U. (2020). Roles of thermokarst lakes in a warming world. *Trends in Microbiology*, *28*(9), 769–779. https://doi.org/10.1016/j.tim.2020.04.002

Jansson, M., Karlson, J., & Jonsson, A. (2012). Carbon dioxide supersaturation promotes primary production in lakes. *Ecology Letters*, *15*(6), 527–532. https://doi.org/10.1111/j.1461-0248.2012.01762.x

Jorgenson, M. T., Harden, J., Kanevskiy, M., O'Donnell, J., Wikland, K., Ewing, S., et al. (2013). Reorganization of vegetation, hydrology, and soil carbon after permafrost degradation across heterogeneous boreal landscapes. *Environmental Research Letters*, *8*(3), 035017. https://doi.org/10.1088/1748-9326/8/3/035017

Kohn, M. J. (2010). Carbon isotope compositions of terrestrial C_3 plants as indicators of (paleo)ecology and (paleo)climate. *PNAS*, *107*(46), 19691–19695. https://doi.org/10.1073/pnas.1004933107

Kuhn, M. A., Thompson, L. M., Winder, J. C., Braga, L. P. P., Tanentzap, A. J., Bastviken, D., & Olefeldt, D. (2021). Opposing effects of climate and permafrost thaw on CH_4 and CO_2 emissions from northern lakes. *AGU Advances*, *2*(4), e2021AV000515. https://doi.org/10.1029/2021AV000515

Kurek, J., Kirk, J. L., Muir, D. C. G., Wang, X., Evans, M. S., & Smol, J. P. (2013). Legacy of a half century of Athabasca oil sands development recorded by lake ecosystems. *Proceedings of the National Academy of Sciences*, *110*(5), 1761–1766. https://doi.org/10.1073/pnas.1217675110

Li, W., Yan, D., Weng, B., & Zhu, L. (2023). Research progress on hydrological effects of permafrost degradation in the Northern Hemisphere. *Geoderma*, *438*, 116629. https://doi.org/10.1016/j.geoderma.2023.116629

Luckman, B. H. (2000). The Little Ice Age in the Canadian Rockies. *Geomorphology*, *32*(3–4), 357–384. https://doi.org/10.1016/S0169-555X(99)00104-X

Martinez-Cruz, K., Sepulveda-Jauregui, A., Walter Anthony, K., & Thallaso, F. (2015). Geographic and seasonal variation of dissolved methane and aerobic methane oxidation in Alaskan lakes. *Biogeosciences*, *12*(15), 4213–4243. https://doi.org/10.5194/bg-12-4595-2015

Marwick, T. R., Tamooh, F., Teodoru, C. R., Borges, A. V., Darchambeau, F., & Bouillon, S. (2015). The age of river-transported carbon: A global perspective. *Global Biogeochemical Cycles*, *29*(2), 122–137. https://doi.org/10.1002/2014GB004911

Matveev, A., Laurion, I., & Vincent, W. F. (2018). Methane and carbon dioxide emissions from thermokarst lakes on mineral soils. *Arctic Science*, *4*, 584–604. https://doi.org/10.1139/as-2017-0047

Meredith, M., Sommerkorn, M., Cassota, S., Derksen, C., Ekaykin, A., Hollowed, A., et al. (2019). Polar regions. In H.-O. Portner, D. C. Roberts, V. Masson-Delmotte, P. Zhai, M. Tignor, E. Poloczanska, et al. (Eds.), *IPCC Special Report on the Ocean and Cryosphere in a Changing Climate* (pp. 1–173). IPCC, WMO, UNEP.

Milkov, A. V., & Etiope, G. (2018). Revised genetic diagrams for natural gases based on a global dataset of >20,000 samples. *Organic Geochemistry*, *125*, 109–120. https://doi.org/10.1016/j.orggeochem.2018.09.002

Nydahl, A. C., Wallin, M. B., & Weyhenmeyer, G. A. (2020). Diverse drivers of long-term pCO_2 increases across thirteen boreal lakes and streams. *Inland Waters*, *10*(3), 360–372. https://doi.org/10.1080/20442041.2020.1740549

Obu, J., Westermann, S., Bartsch, A., Berdnikov, N., Christiansen, H. H., Dashtseren, A., et al. (2019). Northern Hemisphere permafrost map based on TTOP modelling for 2000–2016 at 1 km^2 scale. *Earth-Science Reviews*, *193*, 299–316. https://doi.org/10.1016/j.earscirev.2019.04.023

Ogden, E. L., Cumming, S. G., Smith, L., Turetsky, M. R., & Baltzer, J. L. (2023). Permafrost thaw induces short-term increase in vegetation productivity in northwestern Canada. *Global Change Biology*, *29*(18), 5352–5366. https://doi.org/10.1111/gcb.16812

Olefeldt, D., Heffernan, L., Jones, M. C., Sannel, A. B. K., Treat, C. C., & Turetsky, M. R. (2021). Permafrost thaw in northern peatlands: Rapid changes in ecosystem and landscape functions. In J. G. Canadell & R. B. Jackson (Eds.), *Ecosystem collapse and climate change*, *Ecological studies* (Vol. 241, pp. 27–67). Springer. https://doi.org/10.1007/978-3-030-71330-0_3

Pace, M. L., & Prairie, Y. T. (2005). Respiration in Lakes. In P. A. del Giorgio & P. J. B. Williams (Eds.), *Respiration in aquatic ecosystems* (pp. 103–121). Oxford University Press. https://doi.org/10.1093/acprof:oso/9780198527084.003.0007

Parkhurst, D. L., & Appelo, C. A. J. (1999). Description of input and examples for PHREEQC Version 3.5.0.14000: A computer program for speciation, batch-reaction, one-dimensional transport, and inverse geochemical calculations.

Petermann, E., Gibson, J. J., Knoller, K., Pannier, T., Weiss, H., & Schubert, M. (2018). Determination of groundwater exchange rates and water residence time of groundwater-fed lakes based on stable isotopes of water (^{18}O, ^{2}H) and radon (^{222}Rn) mass balances. *Hydrological Processes*, *32*(6), 805–816. https://doi.org/10.1002/hyp.11456

Peters, D. L., Watt, D., Devito, K., Monk, W. A., Shrestha, R. R., & Baird, D. J. (2022). Changes in geographical runoff generation in regions affected by climate and resource development: A case study of the Athabasca River. *Journal of Hydrology: Regional Studies*, *39*, 100981. https://doi.org/10.1016/j.ejrh.2021.100981

Quinton, W. L., Hayashi, M., & Chasmer, L. E. (2009). Peatland hydrology of discontinuous permafrost in the Northwest Territories: Overview and synthesis. *Canadian Water Resources Journal/Revue Canadienne Des Ressources Hydriques*, *34*(4), 311–328. https://doi.org/10.4296/cwrj3404311

Quinton, W. L., Hayashi, M., & Chasmer, L. E. (2011). Permafrost-thaw-induced land-cover change in the Canadian subarctic: Implications for water resources. *Hydrological Processes*, *25*(1), 152–158. https://doi.org/10.1002/hyp.7894

RAMP. (2005). *Regional Aquatics Monitoring Program 2005*. Standard Operating Procedures (p. 78). Hatfield Consultants. Retrieved from http://www.ramp-alberta.org/

Salmi, T., Määttä, A., Anttila, P., Ruoho-Airola, T., & Amnell, T. (2002). *Detecting trends of annual values of atmospheric pollutants by the Mann-Kendall test and Sen's slope estimates – The Excel template application MAKESENS*. Publications on Air Quality No. 31, Report code FMI-AQ-31 (p. 35). Finnish Meteorological Institute.

Saltzman, M. R., & Thomas, E. (2012). Carbon isotope stratigraphy. In F. M. Gradstein, J. G. Ogg, M. Schmitz, & G. Ogg (Eds.), *The geologic time scale* (pp. 207–232). https://doi.org/10.1016/B978-0-444-59425-9.00011-1

Schmidt, A., Gibson, J. J., Santos, I. R., Shubert, M., Tattrie, K., & Weiss, H. (2010). The contribution of groundwater discharge to the overall water budget of lakes in Alberta/Canada estimated from a radon mass balance. *Hydrology and Earth Systems Sciences*, *14*(1), 79–89. https://doi.org/10.5194/hess-14-79-2010

Schuur, E. A. G., Abbott, B. W., Commane, R., Ernakovich, J., Euskirchen, E., Hugelius, G., et al. (2022). Permafrost and climate change: Carbon cycle feedbacks from the warming Arctic. *Annual Review of Environment and Resources*, *47*(1), 343–371. https://doi.org/10.1146/annurev-environ-012220-011847

Schuur, E. A. G., McGuire, A. D., Romanovsky, V., Schädel, C., & Mack, M. (2018). Chapter 11: Arctic and boreal carbon. In N. Cavallaro, G. Shrestha, R. Birdsey, M. A. Mayes, R. G. Najjar, S. C. Reed, et al. (Eds.), *Second State of the Carbon Cycle Report (SOCCR2): A Sustained Assessment Report* (pp. 428–468). U.S. Global Change Research Program. https://doi.org/10.7930/SOCCR2.2018.Ch11

Schuur, E. A. G., McGuire, A. D., Schädel, C., Grosse, G., Harden, J. W., Hayes, D. J., et al. (2015). Climate change and the permafrost carbon feedback. *Nature*, *520*(7546), 171–179. https://doi.org/10.1038/nature14338

Schuur, T., & Hugelius, G. (2016). In J. Richter-Menge, J. E. Overland, & J. Mathis (Eds.), *Terrestrial carbon cycle. Arctic Report Card 2016*. Retrieved from http://www.arctic.noaa.gov/Report-Card

Smerdon, B. D., Devito, K. J. U., & Mendoza, C. A. (2005). Interaction of groundwater and shallow lakes on outwash sediments in the sub-humid Boreal Plains of Canada. *Journal of Hydrology*, *314*(1–4), 246–262. https://doi.org/10.1016/j.jhydrol.2005.04.001

Smith, L. C., Sheng, Y., MacDonald, G. M., & Hinzman, L. D. (2005). Disappearing Arctic lakes. *Science*, *308*(5727), 1429. https://doi.org/10.1126/science.1108142

Spence, C., Norris, M., Bickerton, G., Bonsal, B. R., Brua, R., Culp, J. M., et al. (2020). The Canadian water resource vulnerability index to permafrost thaw (CWRVIPT). *Arctic Science*, *6*(4), 437–462. https://doi.org/10.1139/as-2019-0028

Summers, J. C., Kurek, J., Kirk, J. L., Muir, D. C. G., Wang, X., Wiklund, J. A., et al. (2016). Recent warming, rather than industrial emissions of bioavailable nutrients, is the dominant driver of lake primary production shifts across the Athabasca oil sands region. *PLoS One*, *11*(5), e0153987. https://doi.org/10.1371/journal.pone.0153987

Sun, W., Zhang, T., Clow, G. D., Sun, Y.-H., Zhao, W.-Y., Liang, B.-B., et al. (2022). Observed permafrost thawing and disappearance near the altitudinal limit of permafrost in the Qilian Mountains. *Advances in Climate Change Research*, *13*(5), 642–650. https://doi.org/10.1016/j.accre.2022.08.004

Turetsky, M. R., Abbott, B. W., Jones, M. C., Anthony, K. W., Olefeldt, D., Schuur, E. A. G., et al. (2019). Permafrost collapse is accelerating carbon release. *Nature*, *569*(7754), 32–34. https://doi.org/10.1038/d41586-019-01313-4

Vitt, D. H., Halsey, L. A., & Zoltai, S. C. (1994). The bog landforms of continental western Canada in relation to climate and permafrost patterns. *Arctic and Alpine Research*, *26*, 1–13. https://doi.org/10.1080/00040851.1994.12003032

Vitt, D. H., Halsey, L. A., & Zoltai, S. C. (2000). The changing landscape of Canada's western boreal forest. *Canadian Journal of Forest Research*, *30*(2), 283–287. https://doi.org/10.1139/x99-214

Vonk, J. E., Tank, S. E., Bowden, W. B., Laurion, I., Vincent, W. F., Alekseychik, P., et al. (2015). Reviews and syntheses: Effects of permafrost thaw on Arctic aquatic ecosystems. *Biogeosciences*, *12*(23), 7129–7167. https://doi.org/10.5194/bg-12-7129-2015

Walvoord, M. A., & Kurylyk, B. L. (2016). Hydrologic impacts of thawing permafrost – A review. *Vadose Zone Journal*, *15*(6), 1–20. https://doi.org/10.2136/vzj2016.01.0010

Walvoord, M. A., & Streigl, R. G. (2021). Complex vulnerabilities of the water and aquatic carbon cycles to permafrost thaw. *Frontiers in Climate*, *3*, 730402. https://doi.org/10.3389/fclim.2021.730402

Walvoord, M. A., & Striegl, R. G. (2007). Increased groundwater to stream discharge from permafrost thawing in the Yukon River basin: Potential impacts on lateral export of carbon and nitrogen. *Geophysical Research Letters*, *34*(12), L12402. https://doi.org/10.1029/2007GL030216

Walvoord, M. A., Voss, C. I., & Wellman, T. P. (2012). Influence of permafrost distribution on groundwater flow in the context of climate-driven permafrost thaw: Example from Yukon Flats Basin, Alaska, USA. *Water Resources Research*, *48*(7), W07524. https://doi.org/10.1029/2011WR01159

Wan, C., Gibson, J. J., & Peters, D. L. (2020). Isotopic constraints on water balance of tundra lakes and watersheds disturbed by permafrost degradation in the Mackenzie Delta region, Northwest Territories, Canada. *Science of the Total Environment*, *731*, 139176. https://doi.org/10.1016/j.scitotenv.2020.139176

Wan, C., Gibson, J. J., Shen, S., Yi, P., & Yu, Z. (2019). Using stable isotopes paired with tritium analysis to assess thermokarst lake water balances in the Source Area of the Yellow River, northeastern Qinghai-Tibet Plateau, China. *Science of the Total Environment*, *689*, 1276–1292. https://doi.org/10.1016/j.scitotenv.2019.06.427

Watmough, S., Whitfield, C., & Fenn, M. (2014). The importance of atmospheric base cation deposition for preventing soil acidification in the Athabasca Oil Sands Region of Canada. *Science of the Total Environment*, *493*, 1–11. https://doi.org/10.1016/j.scitotenv.2014.05.110

Webb, E. E., Liljedahl, A. K., Cordeiro, J. A., Loranty, M. M., Witharana, C., & Lichstein, J. W. (2022). Permafrost thaw drives surface water decline across lake-rich regions of the Arctic. *Nature Climate Change*, *12*(9), 841–846. https://doi.org/10.1038/s41558-022-01455-w

Western Resource Solutions. (2006). Critical loads of acidity to lakes in the Athabasca Oil Sands Region - Modification of the Henriksen model for lake organic content. Final report to: NO_x-SO_x Management Working Group.

Whitfield, C. J., Aherne, J., Gibson, J. J., Seabert, T. A., & Watmough, S. A. (2010). The spatial and temporal geochemical analysis of three boreal peatland complexes. *Hydrological Processes*, *24*(15), 2143–2155. https://doi.org/10.1002/hyp.7637

Whitfield, C. J., Aherne, J., & Watmough, S. A. (2009). Predicting the partial pressure of carbon dioxide in boreal lakes. *Canadian Water Resources Journal*, *34*(4), 415–426. https://doi.org/10.4296/cwrj3404415

Whitfield, C. J., Aherne, J., Watmough, S. A., & McDonald, M. (2010). Estimating the sensitivity of forest soils to acid deposition in the Athabasca Oil Sands Region, Alberta. *Journal of Limnology*, *69*(SUPPL. 1), 201–208. https://doi.org/10.3274/JL10-69-S1-20

Whiticar, M. J., Faber, E., & Schoell, M. (1986). Biogenic methane formation in marine and freshwater environments: CO_2 reduction vs. Acetate fermentation—Isotope evidence. *Geochimica et Cosmochimica Acta*, *50*(5), 693–709. https://doi.org/10.1016/0016-7037(86)90346-7

Wieder, R. K., Vile, M. A., Vitt, D. H., Scott, K. D., Xu, B., Quinn, J. C., & Albright, C. M. (2022). Can plant or lichen natural abundance ^{15}N ratios indicate the influence of oil sands N emissions on bogs. *Journal of Hydrology: Regional Studies*, *40*, 101030. https://doi.org/10.1016/j.ejrh.2022.101030

Wright, S. N., Thompson, L. M., Olefeldt, D., Connon, R. F., Carpino, O. A., Beel, C. R., & Quinton, W. L. (2022). Thaw-induced impacts on land and water in discontinuous permafrost: A review of the Taiga Plains and Taiga Shield, northwestern Canada. *Earth-Science Reviews*, *232*, 104104. https://doi.org/10.1016/j.earscirev.2022.104104

Zabel, N. A., Soliguin, A. M., Wiklund, J. A., Birks, S. J., Gibson, J. J., Fan, X., et al. (2021). Paleolimnological assessment of past hydro-ecological variation at a shallow hardwater lake in the Athabasca Oil Sands Region before potential onset of industrial development. *Journal of Hydrology Regional Studies*, *39*, 100977. https://doi.org/10.1016/j.ejrh.2021.100977

Zastruzny, S. F., Ingeman-Nielsen, T., Zhang, W., & Elberling, B. (2023). Accelerated permafrost thaw and increased drainage in the active layer: Responses from experimental surface alteration. *Cold Regions Science and Technology*, *212*, 103899. https://doi.org/10.1016/j.coldregions.2023.103899